Journal of Applied Phycology
https://doi.org/10.1007/s10811-026-03850-8

RESEARCH

Bioremediation of ozone-produced oxidants in marine RAS using *Ulva ohnoi*: benefits and impacts on seaweed physiology and associated microbiomes

Sabine Weidlich[1] · Clara Priemer[2,3] · Tania Aires[4] · Martin Brenner[2,5] · Wolfram Weckwerth[2,6] · Aschwin Engelen[4] · Andreas Kunzmann[1]

Received: 28 September 2025 / Revised: 10 March 2026 / Accepted: 18 March 2026

Abstract

Maintaining good water quality is essential to the success of recirculating aquaculture systems (RAS). Among water treatment tools, ozone (O_3) has garnered interest from aquafarmers worldwide due to its various beneficial effects. Beyond its germicidal properties, ozone improves solid removal, oxidises toxic nitrogen compounds, and degrades a broad spectrum of biogenic and artificial molecules. However, the ozonation of seawater produces by-products ('ozone-produced oxidants' (OPO)), which can pose significant risks to animal health. In this experiment, we evaluated the capacity of the seaweed *Ulva ohnoi* to bioremediate OPO in an Integrated Multi-Trophic Aquaculture (IMTA)–RAS setup cultivating gilthead seabream (*Sparus aurata*). Effluent water was ozonated and then passed through a cultivation unit containing *U. ohnoi*. OPO concentrations in the water were measured before and after the seaweed unit, and the reduction in OPO was compared to control systems without *U. ohnoi*. Additionally, we assessed the effects of OPO on growth, metabolic composition, photosynthetic efficiency, and associated microbiomes of *U. ohnoi* by comparing seaweed exposed to ozonated water with controls grown without ozonation. The results showed that *Ulva*-containing systems achieved an 11% higher reduction in OPO than controls. However, OPO induced oxidative stress in *U. ohnoi,* leading to reduced growth, altered morphology, and elevated levels of chlorophyll, phenolic compounds, soluble sugars, and selected amino acids. The microbiome associated with *U. ohnoi* shifted, with a reduction in complex carbohydrate-metabolising bacteria. This study demonstrates that *U. ohnoi* can reduce OPO concentrations in marine RAS, but with impacts on the chemical composition, morphology, and microbiome of the seaweed.

Keywords Chlorophyceae · Algae cultivation · Ozone · IMTA · Metabolomics · Phycosphere · Seaweed microbiome

✉ Sabine Weidlich
sabine.weidlich@leibniz-zmt.de

1 Leibniz Centre for Tropical Marine Research (ZMT), Fahrenheitstrasse 6, 28359 Bremen, Germany

2 Molecular Systems Biology, Department of Functional and Evolutionary Ecology, University of Vienna, Djerassiplatz 1, 1030 Vienna, Austria

3 Terrestrial Ecosystem Research, Centre for Microbiology and Environmental System Science, University of Vienna, Djerassiplatz 1, 1030 Vienna, Austria

4 Marine Microbial Ecology & Biotechnology, CCMar, Universidade Do Algarve, Campus de Gambelas, 8100-139 Faro, Portugal

5 Department of Pharmaceutical Sciences/Pharmacognosy, Faculty of Life Sciences, University of Vienna, Josef-Holaubek-Platz 2, Vienna, Austria

6 Vienna Metabolomics Center (VIME), University of Vienna, Djerassiplatz 1, 1030 Vienna, Austria

Introduction

The maintenance of good water quality is crucial in recirculating aquaculture systems (RAS). Ozone (O_3) is widely used in aquaculture due to its strong oxidative capacity, which enables rapid removal of fine suspended solids, dissolved organic matter, and biogenic compounds, improving water clarity, and enhancing downstream biofiltration performance. In addition, ozone effectively inactivates bacterial pathogens, thereby reducing disease pressure and improving animal health (Scolding et al., 2012; Jhunkeaw et al., 2021; Sitthi et al., 2024). Gaseous ozone is commonly produced on-site with ozone generators and mixed into the water to achieve the desired effects through a powerful oxidation process. As a result, ozone has become an important tool for intensifying production, increasing system carrying capacity, and reducing water exchange in marine RAS. However,

Published online: 20 April 2026

the application of ozone-based water purification in marine aquaculture systems presents challenges that require thorough assessment and effective solutions. Seawater contains significant amounts of halogens such as bromine, iodine, and chlorine, which are oxidised by ozone into halo-oxides (Schroeder et al. 2011). Among these, halo-bromines, including hypobromite (OBr^-), hypobromous acid (HOBr), bromamines (NH_2Br, $NHBr_2$, NBr_3), and bromate (BrO_3^-), constitute the majority, but some hypochlorite (ClO^-) and hypochlorous acid (HClO) are also formed (Hoigné et al., 1985). Collectively, these oxidised halogen compounds are referred to as 'ozone-produced oxidants' (OPO). OPO return to their reduced state by oxidising compounds in the water and are therefore transient in nature. However, they can accumulate when ozone is applied excessively or when water is recirculated. Elevated OPO levels have been shown to compromise the health of aquaculture organisms when certain thresholds are exceeded (Reiser et al. 2010; Schroeder et al. 2010; Li et al. 2014), and safe concentration levels for most aquaculture organisms are still unknown. While only very few studies have explored OPO reduction strategies in marine aquaculture such as removal using activated carbon and UV light (Schroeder et al. 2011; Camera-Roda et al. 2019), to date we are not aware of any published research that has investigated bioremediation approaches.

Ulva is a predominantly marine genus of green algae with a cosmopolitan distribution along coastal regions. Most species exhibit a simple thallus structure composed of only three cell types, organised either as a single layer or bilayers (De Clerck et al. 2018; Mantri et al. 2020). Their often leaf-like appearance has earned them the popular name 'sea lettuce'. In natural environments, *Ulva* has garnered attention due to its ability to form massive blooms, commonly referred to as 'green tides', which are typically associated with eutrophication (Teichberg et al. 2010; Van Alstyne et al. 2015). Its general hardiness, the availability of axenic cultures, and a fully sequenced genome have made *Ulva* a popular model organism in laboratory research. Furthermore, *Ulva* has been recognised as a promising candidate for commercial aquaculture within the European Union (Bolton et al. 2016; Steinhagen et al. 2021). Among the various marine algae attracting attention as potential crops for aquaculture in Europe, *Ulva* stands out for several compelling reasons. Its rapid carbon sequestration, resulting in high biomass production, ease of cultivation, high protein and carbohydrate content, and an array of bioactive compounds suitable for medicinal, cosmetic, and nutritional applications, have positioned it as a valuable focus for both research and industry (Bruhn et al. 2011; Hafting et al. 2015; Barzkar et al. 2019; Trigo et al. 2021; Steinhagen et al. 2022). *Ulva* has been demonstrated to be an excellent candidate for Integrated Multitrophic Aquaculture (IMTA) (Chopin et al. 2001), an approach where high- and low-trophic organisms are co-cultivated in systems that promote greater biodiversity compared to traditional monocultures. In these systems, lower-trophic species, such as *Ulva*, can utilise the waste products of higher-trophic organisms (Chopin et al. 2008; Chopin & Tacon 2021). *Ulva*'s nutritional value is comparable, or even exeeds, that of many major land crops (Simon et al. 2022), yet its biomass is highly responsive to environmental conditions. Changes in temperature, salinity, pH, pCO_2 levels, and nutrient availability can impact its metabolic profile, and farming conditions may further influence its physiological performance (Angell et al. 2015; Calheiros et al. 2019, 2021; Chatzoglou et al. 2020; El-Sayed et al. 2022; Van Alstyne & Borgen, 2024). Given this sensitivity to environmental and culturing conditions, *Ulva*'s role as a bioremediator should therefore be carefully evaluated.

More recently, increasing attention has been directed toward the role of seaweed-associated microbiomes in mediating host stress responses, emphasising the need to consider seaweeds as holobionts when investigating their ecophysiology (Dittami et al. 2016; Ghaderiardakani et al. 2020; Hmani et al. 2024). The seaweed-associated microbial communities actively exchange nutrients with their host, act as an interface with the environment, and provide protection against fouling (Egan et al. 2013; Singh & Reddy 2014). The *Ulva* holobiont is one of the most extensively studied seaweed-microbe consortia, and has emerged as a model for investigating seaweed-microbe interactions (Wichard et al. 2015; Wichard 2023). A notable discovery in recent decades is *Ulva*'s dependency on two bacterial genera, *Maribacter* and *Roseovarius*, for the development of its thallus-like morphology (Spoerner et al. 2012; Wichard et al. 2015). Studies have shown that seaweed microbiomes shift with natural environmental gradients (Loos et al. 2024a, b) and are susceptible to changes in temperature (Mars Brisbin et al. 2023), pH (Nevarez-Flores et al. 2024), salinity (Klein Jan et al. 2017), and nutrient regime (Estoup et al. 2024), but a core microbiome releasing algal growth and morphogenesis-promoting bacteria remained stable, for example, in *Ulva compressa* exposed to micropollutants such as antibiotics and endocrine disruptors (Hardegen et al. 2025). However, the impacts of ozonation and ozone-produced oxidants on the microbiome of *Ulva* in mariculture remain unexplored to date, but could have important implications for its cultivation in land-based systems with ozone-based water treatment methods.

We hypothesised that *U. ohnoi* co-cultivated with seabream in an IMTA system could reduce OPO concentrations that accumulate during ozone-based water treatment by acting as a target for the oxidative properties of OPO, potentially mitigating negative impacts associated with residual oxidants and supporting more sustainable ozone use in aquaculture. As all species produced in IMTA contribute to economic revenue, we investigated whether using *U. ohnoi* as a

bioremediator of OPO would alter seaweed biomass quality by shifting primary and secondary metabolite pools as a result of an oxidative stress response, with potential implications for its nutritional value and suitability for downstream applications as a cultivated biomass. Finally, we anticipated that seaweed-associated microbiomes, essential for the functioning of the seaweed, would be affected by OPO through degradation of the *Ulva*-associated biofilm and direct germicidal effects within the phycosphere, potentially altering microbe-mediated functions important for *Ulva* growth, resilience, and cultivation performance. To test these hypotheses, we compared OPO concentrations in the effluent waters of *Ulva*-containing and control setups without seaweed. *Ulva* productivity and photosynthetic efficiency were monitored to assess the alga's physiological responses to OPO exposure. Focussed GC–MS metabolomics was applied to quantify shifts in key primary metabolite pools, providing insight into *Ulva*'s oxidative stress responses and potential impacts on biomass quality. In addition, targeted assays were performed to quantify chlorophyll, phenolic compounds, and soluble sugars, complementing the metabolomic profile and linking biochemical and morphological changes to biomass composition and nutritional quality. In parallel, 16S rRNA gene metabarcoding was used to characterise seaweed-associated microbiomes, providing first insights into how OPO influence organism-associated surface biofilms and the composition of microbial communities associated with *U. ohnoi*. In this study, the term 'ozone-produced oxidants' (OPO) is used to denote total residual oxidant (TRO) concentrations, measured spectrophotometrically as Cl_2 equivalents.

Materials and methods

Algae material collection & cultivation

Ulva was collected from the sedimentation tanks of experimental aquaculture ponds growing Gilthead seabream (*Sparus aurata*) and European seabass (*Dicentrarchus labrax*) at the biological station EPPO (Estação Piloto de Piscicultura de Olhão) in Olhão, Portugal, and transported to the experimental site in Alvor in buckets protected from light and in cool conditions. Thalli consisted of smooth, laminar fronds with a light green coloration. The seaweed was cleaned from epibionts and small animals and distributed to the cultivation units one week before the beginning of the experiment for acclimation. Samples were taken before starting the experiment.

Experimental setup

Each experimental unit consisted of a 450-L conical PVC fish tank stocked with 18 gilthead seabream (100–150 g), connected in series to a water treatment compartment comprising two 80-L rectangular PVC tanks (Fig. 1). The first water treatment tank, located immediately downstream of the fish tank, contained a mechanical filter (25 µm) and a protein skimmer (Deltec i450, Deltec, Germany). Ozone was generated on-site by an ozone generator (AquaMedic ozone 90, AquaMedic, Germany) from pure O_2 and fed into the skimmer through the pump air inlet. In ozone-treated units, OPO concentrations were monitored via a redox sensor and controller (Sander, Germany), maintaining 500–600 mV, corresponding to 0.238–0.567 mg L^{-1} Cl_2 equivalents as measured by the DPD method. In the controls, the skimmers worked on air. The second water treatment tank contained *U. ohnoi* with an initial biomass of 0.5 g L^{-1}, resulting in a seaweed-to-fish ratio of 1:10. Fish and seaweed densities were lower than typical commercial stocking densities for intensive tank culture, but the initial biomass ratio was only slightly below previously reported IMTA co-cultivation setups involving *Ulva* and finfish, and was well within the range after 7 days (Pintado et al. 2023; Batır et al. 2024; Cesare Marincola et al. 2025). Each *Ulva* cultivation tank was equipped with a perforated air tube along the tank bottom to create water movement. Fish tanks were shaded from sunlight by a plastic canvas. Water was pumped from the coastal lagoon Ria de Alvor first into a shaded reservoir of 200 m^3, and then flowed into the fish tanks and from there into the water treatment compartments at a mean rate of 1.835 L min^{-1} (138% h^{-1}), comparable to flow rates reported in similar land-based IMTA co-cultivation studies (e.g., Batır et al. 2024). To avoid exposing the seabreams in our setup to potentially toxic concentrations of OPO, water was not recirculated into the fish tanks, but collected in a

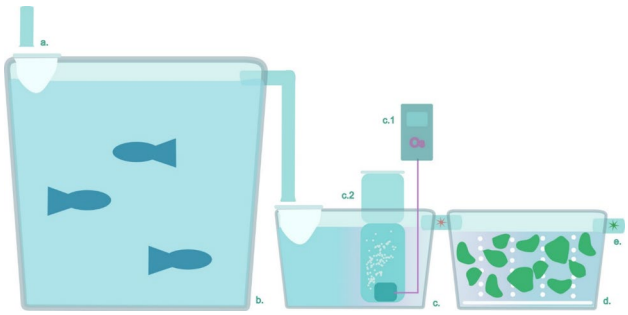

Fig. 1 Experimental setup. The experimental IMTA setup consisted of **a**.) an inlet supplying the system with water pumped from the Ria de Alvor (PT), **b**). a 450-L conical PVC tank stocked with 18 gilthead seabream (*S. aurata*), **c**.) an 80-L rectangular water treatment unit with c.1). an ozone generator supplied with pure O_2 and c.2). a protein skimmer mixing the ozone into the effluent water, **d**.) an 80-L seaweed cultivation unit with a perforated plastic tube at the bottom bubbling air for water movement growing *U. ohnoi*, **e**.) an outlet. The system was operated as a flow-through. Water samples for OPO measurements were taken upstream (red star) and downstream (green star) of the *Ulva* unit

dedicated retention tank where residual OPO were allowed to degrade naturally through reaction with dissolved organic matter before final disposal (Fig. 1).

Experimental design

We tested the capacity of *U. ohnoi* to act as an OPO biofilter, as well as the impacts of OPO on *U. ohnoi* biomass gain, photosynthetic efficiency, biomass and associated microbiomes, using three treatments (n = 3 each): (i) ozone-treated water with *Ulva*, (ii) ozone-treated water without *Ulva*, and (iii) untreated water with *Ulva*. Comparing treatments (i) and (ii) tested whether *Ulva* reduced OPO concentrations, while comparing treatments (i) and (iii) assessed the effects of OPO exposure on algal biomass.

Sampling

Temperature, oxygen and pH were measured on each sampling day between 9 and 11 am using a handheld multisensor (WTW MultiLine Multi 3630, Xylem Analytics, Germany) and the corresponding probes (Fig. S1, Supplemental material). Every 3 days, 10 mL water samples were taken from each *Ulva* tank in- and outflow to determine OPO concentrations using the colorimetric *N,N*-diethyl-p-phenylendiamine (DPD) method following the producer's instructions (Lovibond Water Testing, Germany), with absorbance measured at 530 nm using a Hach photometer (DR3900 Labor-Spektralphotometer, Hach, Germany) and results expressed as mg L^{-1} chlorine equivalents (Cl_2). *Ulva* physiological performance was assessed by measuring the optimal quantum yield (F_v/F_m) using pulse-amplitude modulated fluorometry. Three intact fronds of *Ulva* of comparable size (~ 10 cm in length) were randomly taken from each cultivation unit, carefully blotted to remove excess water, and dark-adapted for 10 min using leaf clips (Walz, Germany). Measurements were performed using a PAM-2500 fluorometer (Walz, Germany) operated with PAM Win 3 software, with the saturating pulse set to Int. = 8, the measuring light for F_0 and F_m set to Int. (F_0,F_m) = 1, and gain and damping both set to 2. Fv/Fm was determined following standard protocols (Maxwell & Johnson 2000).

Biomass production was quantified by removing the entire *Ulva* biomass from each cultivation unit, draining excess water using a centrifuge, and weighing wet biomass to the nearest gram. Biomass gain between sampling days was calculated as the difference between consecutive sampling weights. Samples for molecular content analyses were taken after 1, 7 and 13 days, transported to the lab on ice, and stored at – 80 °C until processing. Samples were freeze-dried (Thermo Fisher Scientific, US) and pulverised in 2 mL Eppendorf tubes using a TissueLyser II (Qiagen, Germany) and tungsten beads. For 16S rRNA gene metabarcoding, *Ulva* tissue samples of 1–2 cm^2 were taken at the start of the experiment and after 1, 7, and 13 days. Samples were placed in 2 mL Eppendorf tubes containing Longmire lysis buffer (Longmire et al. 1997) and transported to the lab on ice. They were stored at 4 °C until extraction. The identity of the *Ulva* species used in the experiment was confirmed by DNA barcoding of the *tuf*A gene (Saunders & Kucera 2010).

Biomolecular assays: Chlorophyll, soluble sugars, phenols, flavonoids and tannins

Photosynthetic pigments, soluble sugars, and phenolic compounds were extracted following the protocol by Preiner et al. (2024). Sequential extractions were carried out by washing the freeze-dried and pulverised plant material with acetone (80%), methanol (80%), and ethanol (80%). The extracts were pooled, and aliquots were divided into Eppendorf tubes stored at – 80 °C.

Chlorophyll *a* and *b* were estimated following the protocol by Wellburn & Lichtenthaler (1984). Pigments were extracted with 80% acetone, and absorbances were measured at 663 and 646 nm with a microplate reader (Tecan Spark, Tecan, Switzerland). Chlorophyll contents were calculated using the formulae:

$$C_a\left(\mu g\ mL^{-1}\right) = 0.7 * \left(12.21 * A_{663} - 2.81 * A_{646}\right)$$

and

$$C_b\left(\mu g\ mL^{-1}\right) = 0.7 * \left(20.13 * A_{646} - 5.03 * A_{663}\right)$$

The values were summed to obtain the total chlorophyll contents.

An estimation of soluble carbohydrates was done following the method of Hansen & Møller (1975). 100 µL of freeze-dried and pulverised *Ulva* tissue was mixed with 200 µL pre-chilled H_2SO_4 (72%) and vortexed. 400 µL of anthrone reagent was added and the mix was heated at 95 °C for 15 min. Samples were cooled on ice, and the absorbance of the green colour complexes were measured within 15 min at 630 nm. A standard curve was prepared with D-glucose in a range of 50 to 3000 nmol mL^{-1}. Results were expressed as mg glucose per g DW (dry weight). Total phenolic compounds were estimated using the Folin–Ciocalteu method, following the protocol by Biju et al. (2014). In short, 100 µL of extract was mixed with the Folin-Ciocalteu reagent to form a blue chromophore, and absorbance was read at 550 nm. A standard was prepared using gallic acid (50–500 µg mL^{-1}), and results were expressed as mg gallic acid equivalents (GAE) per g dry weight. Total flavonoid content was estimated with the aluminium chloride method following the protocol by Chang et al. (2002), modified by Biju et al. (2014). 200 µL of extract were reacted with 10%

$AlCl_3$, which reacts with the hydroxyl- and keto groups of flavones and flavonols, as well as the ortho-dihydroxyl groups in flavonoids. The resulting pink colour complexes were measured photometrically at 510 nm. A standard (20–100 µg mL^{-1}) was prepared using quercetin. Total flavonoid content was expressed as mg quercetin equivalents (QUE) per g DW. Total condensed tannins were estimated with the vanillin method after Broadhurst & Jones (1978). 200 µL of extract were reacted with a 4% vanillin methanol solution. A standard curve was prepared with Catechin (20–100 µg mL^{-1}). The reaction of vanillin with tannins yields a red product, and absorbance was measured at 500 nm. Results were expressed in mg Catechin Equivalents (CE) per g DW.

Metabolomics

The extraction of polar metabolites was carried out following Weckwerth et al. with slight modifications. Ice cold extraction solvent (750 µL) consisting of methanol (LC–MS grade, Merck) chloroform (anhydrous > 99%, Sigma Aldrich), and water (Milli-Q) in a ratio of 2.5:1:0.5 (v/v) was added to approximately 20 mg of freeze-dried and pulverised *Ulva* tissue. A defined volume of 7 µL of a solution of 10 mmol of pentaerythritol (PE) and 10 mM phenyl-β-d-glucopyranoside (PGP) respectively in water (Milli-Q) was added as internal standards. Supernatants were transferred into a 1.5 mL tube (polypropylene) after 20 min of ultrasonication in an ice-cold water bath and subsequent centrifugation (4 min, 4 °C, 14,000 × *g*). As a washing step another 250 µL of extraction solvent was added to the remaining pellet, and the supernatant was combined with the previous one after ultrasonication and centrifugation as described before. Phase separation was induced by the addition of 350 µL of cold water (Milli-Q) to the supernatant. The mixture was briefly and vigorously mixed and centrifuged at 14,000 × *g* for 4 min at 4 °C. From the aqueous upper phase, 900 µL were transferred to a new 1.5 mL tube, and the remaining upper phase of all samples was combined and split into 900 µL aliquots. These were used for method establishment and quality control during GC–MS measurements. All samples and aliquots were dried in a vacuum centrifuge at 30 °C and 0.1 mbar for 5 h and stored at – 80 °C until measurement.

Derivatisation of the dried extracts, measurement and data evaluation was performed as described in Groot Crego et al. (2024) with slight modification of the detector voltage to 1700 V. All samples were run in randomised order and deconvolution, processing of chromatograms and annotation via spectra was performed using ChromaTOF (version 5.55.29.0.1187, LECO Cooperation) and MS-DIAL, (version 4.7) (Tsugawa et al. 2015). Peaks were manually curated before integration. Targeted metabolites were identified by comparison of mass spectra and retention index with authentic standards measured in the same run (SX2_Supplemental_Table_Metabolites_GC-MS). Twenty unknown features were annotated using an external library (Fiehn BinBase DB (Rtx5-Sil MS, predicted Kovats RI) https://systemsomicslab.github.io/compms/msdial/main.html#MSP) according to the metabolomics standards initiative levels of identification. One of the internal standards (penthaerithritol) was used to calculate relative abundances of metabolites and account for errors introduced during extraction. Calibration curves were created from dilution series of the standards for targeted metabolites and used to obtain absolute amounts per amount of dry biomass.

16S rRNA gene metabarcoding

DNA extractions

Extractions were carried out using the Quick-DNA Miniprep Kit Catalog Nos. D3024 & D3025 (Zymo Research Corp). Algal tissue was placed in 2 ml Eppendorf tubes with 100 µL Genomic Lysis- and Beta-Mercapto buffer and 2 tungsten beads per tube. Tissues were lysed for 2 × 5 min at a frequency of 20 Hz per second in a TissueLyser II (Qiagen, Germany). Samples were centrifuged briefly to reduce foam and an additional 400 µL of Beta-Mercapto buffer was added. Samples were vortexed to thoroughly mix the buffer and sample. Samples were centrifuged at 10,000 rpm for 5 min, and further steps of the extraction were carried out following the producer's instructions.

16S rRNA gene metabarcoding

For sequencing, the variable region V3—V4 of the 16S rRNA gene was amplified using the universal primer pair 341 F (5′-CCTACGGGAGGCAGCAG-3′) and 806R (5′-GGACTACHVGGGTWTCTAAT-3′) (Muyzer et al. 1993; Caporaso et al. 2012). PCR products were normalised using the SequalPrep Normalization Plate Kit (Thermo Fischer Scientific, USA), pooled equimolarly and sequenced on the Illumina MiSeq v3 2 × 300 bp (Illumina, USA). Demultiplexing after sequencing was based on 0 mismatches in the barcode sequences. Amplification and sequencing were carried out in the microbiome lab of the IKMB, Kiel University, Germany.

Sequences were processed using Qiime2 (Bolyen et al. 2019). After primer removal with cutadapt (Martin 2011), dada2-plugin was used with default settings to denoise, quality filter and merge demultiplexed raw reads (Callahan et al. 2016). Taxonomic assignments were computed using the feature-classifier plugin (classify sklearn) with default settings and a pre-trained SILVA classifier (release 138) pre-trained with the respective primers for prokaryotes (Pedregosa et al. 2012; Quast et al. 2013; Bokulich et al.

2018). All sequencing data were deposited at the NCBI Sequence Read Archive (SRA) under the accession number PRJNA1356848.

Statistical analyses

OPO lowering capacity and effects on Ulva biomass

All statistical analyses were performed in RStudio (version 2023.6.0.421), using the packages 'vegan' (Oksanen et al., 2024), 'car' (Fox & Weisberg 2019), 'dplyr' (Wickham et al. 2023), 'nlme' (Pinheiro et al. 2018), 'lme4' (Bates et al. 2015), 'ez' (Lawrence 2016), 'emmeans' (Lenth 2021), and 'afex' (Singmann et al. 2024). Data were checked for normality by visual inspection of histograms and Shapiro–Wilk tests, and homogeneity of variance was evaluated by performing Bartlett's or Levene's tests. Data visualisation was done using the 'ggplot2' package (Wickham, 2016).

The effect of ozone treatment on *Ulva* biomass gain was analysed using a linear mixed-effects model with treatment and sampling day as fixed effects and tank ID included as a random intercept. This approach accounts for the non-independence of repeated observations while allowing assessment of treatment effects over time. Models were fitted using restricted maximum likelihood estimation (REML). Post hoc pairwise comparisons were conducted using Tukey's adjustment.

Differences between OPO inflow and outflow concentrations were expressed as percent decline to account for substantial variability in inflow concentrations between treatments and among replicates (*Ulva*: mean = 0.446 ± 0.107 mg L^{-1}; control: mean = 0.406 ± 0.098 mg L^{-1}). A linear mixed-effects model was fitted to assess treatment effects on OPO decline over time, with treatment, sampling day, and their interaction included as fixed effects, and tank ID included as a random intercept to account for repeated measurements within tanks. Pairwise t-tests with Tukey's adjustment for multiple comparisons were performed to show differences at each sampling day.

Photosynthetic efficiency was analysed using a linear mixed-effects model with treatment and sampling day as fixed effects and tank ID as a random intercept to account for repeated measures. To account for heteroscedasticity, a variance structure allowing different variances among each sampling day was included using varIdent (). Models were fitted using REML, and post hoc pairwise comparisons were conducted with Tukey's adjustment.

Chlorophyll, soluble sugars, phenols, flavonoids, and tannins were analysed to test for effects of treatment and sampling day. Repeated measures ANOVA was applied when assumptions of normality and homogeneity of variance were met, otherwise linear mixed-effects models with tank ID as a random intercept were used to account for repeated measures and unequal variance across tanks or sampling points. Sphericity was assessed using Mauchly's test and Greenhouse–Geisser and Huynh–Feldt corrections were applied when necessary. Pairwise post hoc comparisons were performed using Tukey's adjustment for multiple comparisons.

Multivariate patterns of metabolites analysed by GC–MS were explored using Partial Least Squares Discriminant Analysis (PLS-DA) with ozone treatment as the response, allowing visualisation of overall differences in metabolite composition between treatments and across sampling days. The first two components were visualised, with samples colored by treatment and shaped by sampling day, and treatment groups highlighted by ellipses. A Euclidean distance matrix was calculated from the scaled data, and a PERMANOVA was performed to determine the impacts of sampling day and treatment on metabolite composition. Permutations were constrained within tanks to account for repeated measures. Absolute quantities of the metabolites contained in the standard were displayed as box plots. The assumption of normality was violated in six cases, but since the p-values were near 0.05 (0.017–0.038) and ANOVA is considered robust against deviations from normality (Schmider et al., 2010), repeated measures ANOVAs with sampling day (Day 1 – Day 13) and treatment as fixed factors and tank ID as a random factor were used on all metabolites. This approach accounts for the repeated-measures over time and allows reliable testing of treatment effects. Post hoc pairwise t-tests with Bonferroni correction were performed to assess differences for each sampling day.

Microbial community analysis: 16S rRNA gene sequences

All analyses and plots were performed and visualised using RStudio (version 2023.6.0.421) and the 'phyloseq' (McMurdie & Holmes, 2013), 'vegan' (Oksanen et al. 2020), 'car' (Fox & Weisberg 2019), 'dplyr' (Wickham et al. 2023), and 'DESeq2' (Love et al., 2014) packages, along with MicrobiomeAnalyst (Dhariwal et al. 2017). In RStudio, a phyloseq object was created by combining a feature table, a metadata table, and a taxonomy table to enable unified handling of sequencing data and experimental factors. Low abundance reads were filtered (minimum of 2 total counts and 10% prevalence across samples), and 27 mitochondrial and 96 chloroplast sequences were removed. Rarefaction curves were created in MicrobiomeAnalyst to assess sequencing depth sufficiency. Shannon and Simpson diversity indices and Observed richness were calculated in RStudio following rarefaction across samples to evaluate treatment- and time-related changes in microbial diversity. Because diversity data did not meet parametric assumptions, Kruskal tests were used to test for differences in diversity and richness between treatments, and pairwise Dunn tests with Bonferroni correction were performed to test for

differences between treatments on each sampling day while correcting for multiple testing. A Bray–Curtis dissimilarity matrix was calculated on unrarefied ASV counts to preserve all observed taxa, and Principal Coordinates Analysis (PCoA) was used to visualise differences in microbial community composition across sampling days and treatments. PERMANOVA was performed to test for the effects of treatment and sampling day, and for interactions between factors, with permutations restricted within tank ID to account for the repeated-measures design. A bubble plot was created to show the relative abundances of the 15 most abundant families for both treatments across all sampling dates. To identify ASVs significantly associated with ozone treatment, a differential abundance analysis was performed for each sampling day on the complete data set at ASV level. BaseMean abundances, log2fold-changes, and adjusted p-values were exported and the log2fold changes for Day 7 and Day 13 were plotted as horizontal bar charts, displaying baseMean values for each ASV. Core microbiomes for treatment and control were identified to determine persistent microbial taxa resilient to OPO exposure. To this end, a dataset containing all Day 13 samples was imported in MicrobiomeAnalyst and filtered to a minimum count of two and 10% prevalence, and low-variance features (10% interquartile range) were removed to reduce noise. This filtering retained 147 ASVs. Data were then log-transformed, and core taxa were defined based on a relative abundance threshold of 2% and a prevalence of 20% across samples. These thresholds were chosen to identify consistently occurring and ecologically relevant taxa while excluding rare or sporadically detected members unlikely to contribute substantially to community structure. Core microbiome data were then exported and visualised in RStudio.

Results

OPO lowering capacity

OPO concentrations declined in both *Ulva* treatment and control (Fig. 2). In the controls, the reduction ranged between 60 and 82% throughout the experiment. The presence of *Ulva* significantly increased OPO reduction ($t(4) = 5.27$, $p = 0.006$), augmenting the decline by an additional 11.1%. Mean OPO outflow concentrations were consistently lower in *Ulva* systems than in controls across all sampling days (Fig. 2). There was no statistically

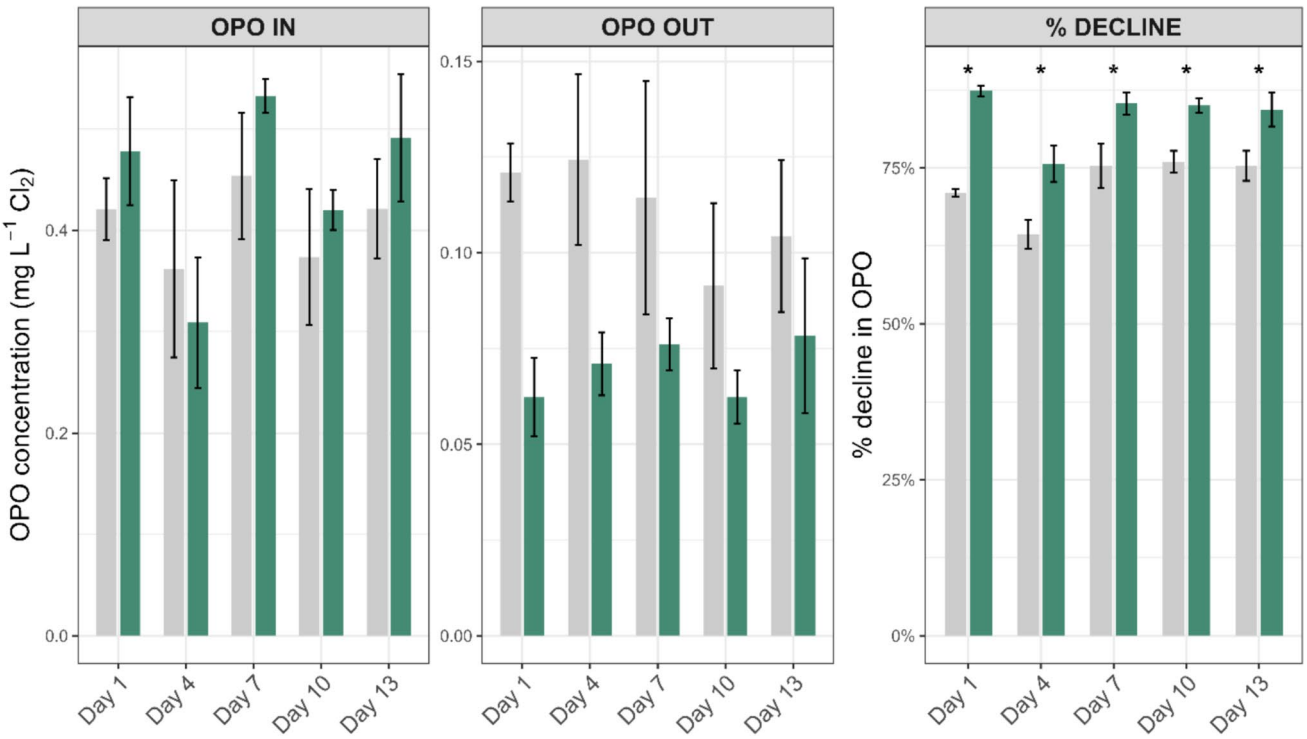

Fig. 2 OPO concentrations in experimental systems. Bar plots show influx (OPO entering the seaweed tanks), outflux (OPO leaving the seaweed tanks), and % decline (percentage reduction of OPO) across five sampling days for control and *Ulva* treatments. Error bars represent standard errors of the mean. In the decline plot, asterisks indicate statistically significant differences between treatments at each sampling day ($p < 0.05$). OPO decline was significantly higher in *Ulva* treatments than in controls ($p = 0.006$). Systems containing *Ulva* are shown in green, while controls without seaweed are shown in grey (*Ulva*: $n = 3$, control: $n = 3$)

significant interaction between treatment and sampling day, suggesting that OPO decline trends over time were constant across treatments.

Morphological changes

One week into the experiment, *Ulva* in ozone treatments began to show morphological differences from the controls (Fig. 3). Ozonated *Ulva* had a darker green coloration and increased rigidity. When placed on a smooth surface, the ozone-treated samples did not flatten out as smoothly as the controls but instead maintained their shape, partly sticking up. The fronds also appeared slightly more ragged than those of the controls (Fig. 3).

Biomass gain

The linear mixed-effects model (fit by REML) revealed a significant negative impact of ozone on biomass gain ($t(4) = -3.37$, $p = 0.028$), with a 29.8% reduction in the ozone treatment compared to the no ozone control group (Fig. 4). Pairwise comparisons for each sampling day showed that biomass gain differed between treatments on Days 4 ($t(4) = 3.37$, $p = 0.028$) and 10 ($t(4) = 4.31$, $p = 0.013$), but not on Day 7, 13 ($t(4) = 2.71$, $p = 0.05$), and 17 ($t(4) = 1.12$, $p = 0.324$; $t(4) = -0.66$, $p = 0.548$). Sampling day had a significant effect on biomass gain ($p < 0.001$), with gains decreasing over time. (Fig. 4).

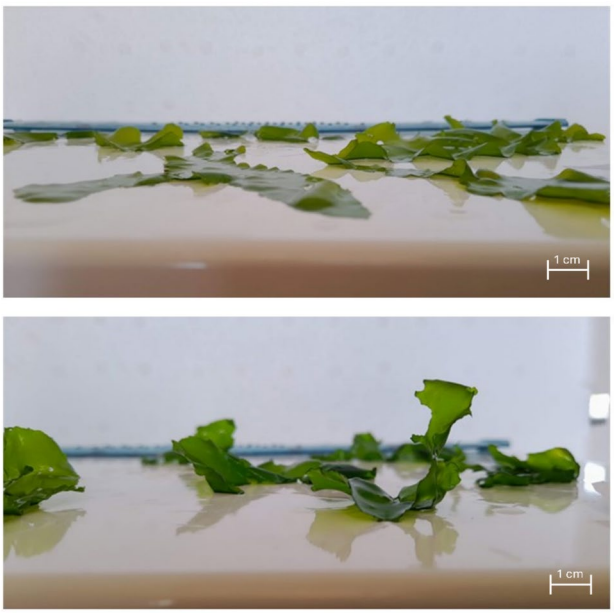

Fig. 3 Morphological changes in ozonated *U. ohnoi*. The upper image shows *Ulva* from the control units (without ozonation), while the lower image displays *Ulva* from ozone-treated systems, exhibiting increased rigidity, reduced flexibility, a darker colour, and a slightly more ragged appearance compared to the controls

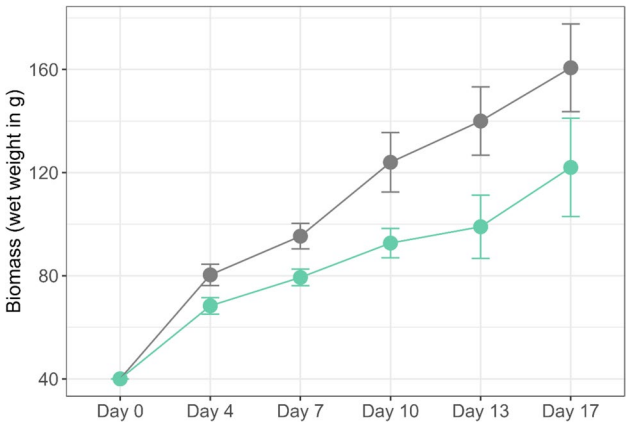

Fig. 4 Biomass measurements. Both ozone treatment (turquoise) and control (grey) systems showed biomass gain throughout the experiment. Ozone had a variable negative effect on *Ulva* growth, with significant impacts observed on Days 4, 10, and 13. Overall, the controls approximately quadrupled their wet weight biomass over 17 days, while ozone-treated systems only tripled their biomass over the same period. Dots represent means, and error bars indicate the standard deviation of the data (ozone: n = 3, control: n = 3)

Photosynthetic efficiency

There was a significant negative effect of ozone treatment ($F(1,4) = 11.53$, $p = 0.027$) on photosynthetic efficiency (F_v/F_m), with pairwise comparisons revealing a significant ($p < 0.05$) difference on Day 4 ($p = 0.037$), but no effect on Days 10 ($p = 0.075$) and 13 ($p = 0.092$) (Fig. 5). Additionally, there was an effect of sampling day ($F(4,16) = 22.36$, $p < 0.001$), but no interaction between factors. However, all measured values after Day 1 remained between 0.7 and 0.8, indicating a generally good health status of *Ulva* in both the ozone and control treatments. (Fig. 5).

Ulva metabolic content analysis

Biomolecular assays: Chlorophyll, soluble carbohydrates, phenols, flavonoids, condensed tannins

Ozone treatment had a positive effect on chlorophyll content ($F(1,4) = 23.53$, $p = 0.008$), with an overall increase of 17.32%. There was also an effect of sampling day ($F(2,8) = 46.38$, $p \leq 0.001$), but no interaction between factors. Post hoc pairwise comparisons of marginal means showed a positive effect of ozone treatment on total chlorophyll on Day 13 ($t(4) = -3.792$, $p = 0.019$), with chlorophyll contents in ozone samples 32.15% higher than in controls. Total phenolic compound concentrations were also higher (+9.81%) in ozonated *Ulva* than in controls ($F(1,4) = 29.56$,

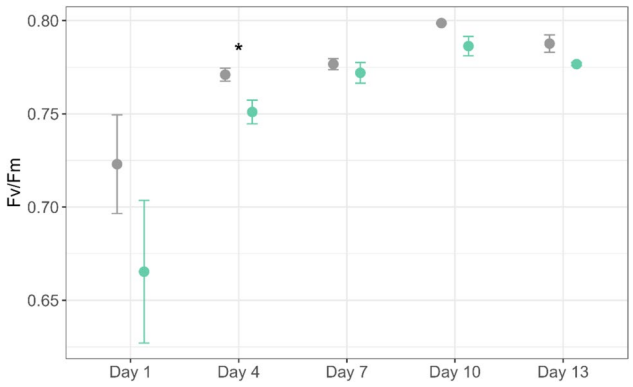

Fig. 5 Photosynthetic Efficiency (F_v/F_m). Mean F_v/F_m values of *Ulva* during several days of ozone exposure measured after 10 min of dark incubation using leaf clips. Ozone had a significant negative effect on F_v/F_m ($p = 0.027$). Dots represent means, and error bars indicate standard errors (SE). Significant differences from pairwise post hoc comparisons are indicated by asterisks. Ozone treatments are shown in turquoise, and controls are shown in grey (ozone: $n = 3$, control: $n = 3$)

$p = 0.006$), but no effect of sampling day was evident. Post hoc comparisons of means showed elevated phenol levels on Day 13 ($t(4) = -5.09$, $p = 0.019$), with 24.22% more phenols in ozone treatments than in controls. Flavonoid content was influenced by ozone treatment (+20.3%; $F(1,4) = 78.7$, $p = < 0.001$) and sampling day ($F(2,8) = 12.62$, $p = 0.003$), with a difference of +34.64% on Day 13 according to post hoc testing ($t(4) = -4.18$, $p = 0.014$). Condensed tannins did not differ between treatments but varied among sampling days ($F(2,8) = 19.07$, $p = 0.001$). Pairwise post hoc testing revealed a difference of +32.09% condensed tannins in ozone treatments on Day 13 ($t(4) = -2.88$, $p = 0.045$). Repeated measures ANOVA did not detect any influence of treatment or sampling day on soluble carbohydrate content ($F(1,4) = 0.59$, $p = 0.485$), but post-hoc testing showed that soluble sugars were significantly higher ($t(4) = -3.08$, $p = 0.037$) in ozone treatments on Day 13, with a difference of +40.85% compared with controls (Fig. 6).

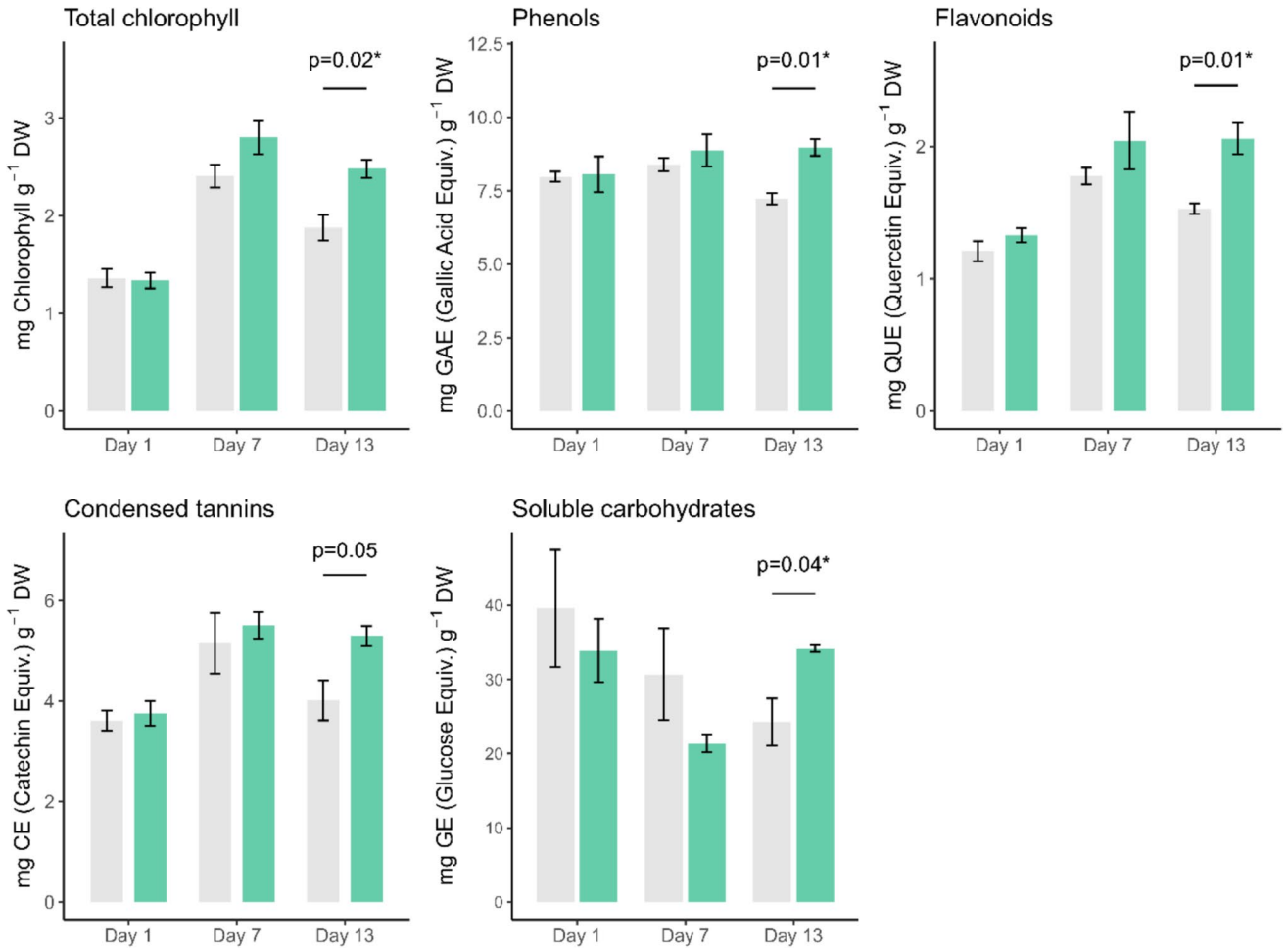

Fig. 6 *Ulva* composition (total chlorophyll, phenols, flavonoids, condensed tannins, and soluble carbohydrates) throughout the experiment in ozone treatment (turquoise) and control (grey) groups. Bars represent means, error bars indicate standard errors (SE). There were overall increases in chlorophyll (+17.32%), phenol (+9.81%) and flavonoid (+20.3%) contents in ozonated *Ulva* compared with controls. P-values are derived from pairwise post hoc comparisons and are rounded to two decimal places. Only p-values ≤ 0.05 are displayed

Metabolomic analysis

Non-targeted analysis of metabolites was performed with gas chromatography coupled to mass spectrometry (GC–MS). PLS-DA of our relative abundance data showed a clear separation between samples of both treatments along PLS-DA Component 1 (Fig. 7). PERMANOVA showed a significant effect of treatment ($F(1, 14) = 1.767$, $p = 0.008$), a significant impact of sampling day ($F(3, 14) = 2.179$, $p = 0.001$), and no interaction between factors ($F(2, 14) = 0.814$, $p = 0.701$; Table 1).

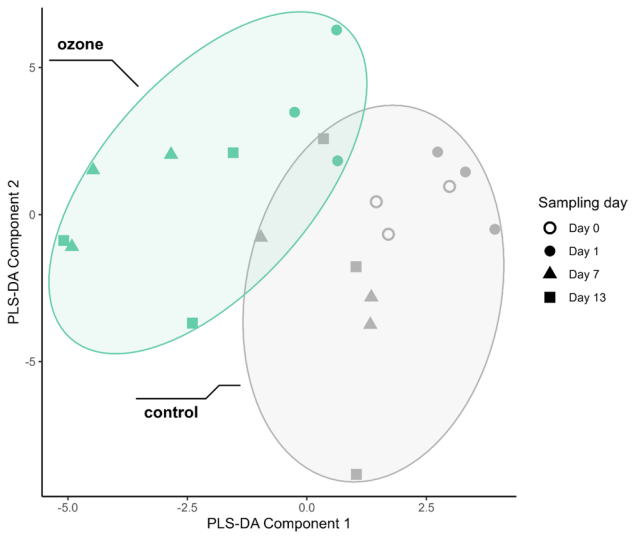

Fig. 7 Partial Least Squares Discriminant Analysis (PLS-DA) of relative metabolite abundance from GC–MS analysis of *Ulva* tissue samples. The plot displays the first two components (PLS-DA Component 1 and 2). Each point represents an individual *Ulva* sample, with colours indicating treatment groups (ozone = turquoise, control = grey). The PLS-DA was performed on the complete scaled metabolite abundance data (relative abundances per unit biomass of 79 identified metabolites). The analysis reveals a clear separation of samples by treatment along Component1

Table 1 PERMANOVA of relative abundance metabolite data from GC–MS analysis of *Ulva* tissues. The table shows the degrees of freedom (DF), sum of squares (SUMOFSQS), R-squared (R^2), F-statistic (F), and p-value (PR(> F)) for the effects of Treatment, Day and the interaction between Treatment and Day

	DF	SUMOFSQS	R^2	F	PR(> F)
TREATMENT	1	79.72	0.074	1.767	0.008**
DAY	3	295.00	0.273	2.179	0.001 ***
TREATMENT* DAY	2	73.57	0.068	0.815	0.701
RESIDUAL TOTAL	14	631.71	0.585		
	20	1080.00	1.000		

Repeated measures ANOVA revealed that seven metabolites quantified through absolute quantification were affected by ozone treatment: glutamine ($p = 0.005$), leucine ($p = 0.008$), proline ($p = 0.041$), serine ($p = 0.004$), threonine ($p = 0.038$), valine ($p = 0.039$) and pyruvic acid ($p = 0.034$). Pairwise t-tests showed statistical differences in metabolite concentrations after 7 and 13 days of ozonation in glutamine ($p = 0.003$, $p = 0.009$), leucine ($p < 0.001$, $p = 0.004$), proline ($p = 0.019$, $p = 0.003$), serine ($p = 0.031$, $p = 0.037$), threonine ($p = 0.05$, $p = 0.004$) and valine ($p = 0.031$, $p = 0.002$). Pyruvic acid was elevated only on Day 1 in ozone treatments ($p < 0.001$). Sampling day had a significant impact on asparagine ($p = 0.011$), aspartic acid ($p = 0.018$), fumaric acid ($p = 0.029$), glutamine ($p = 0.001$), leucine ($p < 0.001$), proline ($p = 0.001$), pyruvic acid ($p = 0.002$), serine ($p = 0.02$), succinic acid ($p = 0.034$), and valine ($p < 0.001$). An interaction between factors existed in leucine ($p = 0.018$), proline ($p = 0.011$) and pyruvic acid ($p = 0.001$): the impact of ozone on proline became more pronounced over time, while pyruvic acid was highly increased in ozone treatments on Day 1 but declined sharply at later time points (Fig. 8).

16S rRNA gene metabarcoding

Sample statistics

The mean number of reads per sample was 13482 with a range of 7062–21675 reads after quality control and filtering. Rarefaction curves plateaued for all samples even after rarefication to the minimum number of reads, indicating sufficient sequencing depth. A total of 231 ASVs were retained after filtering the data set for low abundance reads and a 10% prevalence threshold.

Alpha diversity

There was no significant effect of treatment on Observed richness (Kruskal Wallis, $\chi^2 = 13.6$, $df = 7$, $p = 0.059$), Shannon (Kruskal Wallis, $\chi^2 = 8.81$, $df = 7$, $p = 0.266$) or Simpson indices (Kruskal Wallis, $\chi^2 = 7.28$, $df = 7$, $p = 0.400$) (Fig. 9).

Beta diversity

The PCoA plot based on Bray–Curtis dissimilarities shows the successional divergence of ozone samples from controls. While samples from both treatments clustered closely at Day 0 and Day 1, a differentiation along Axis 1 began to emerge at least from Day 7 onwards (Fig. 10). PERMANOVA analysis confirmed significant differences in community composition between treatment and control, explaining 18.3% of the observed variance, and across sampling days (28.3%), with a strong interaction between the two factors (25.5%; Table 2).

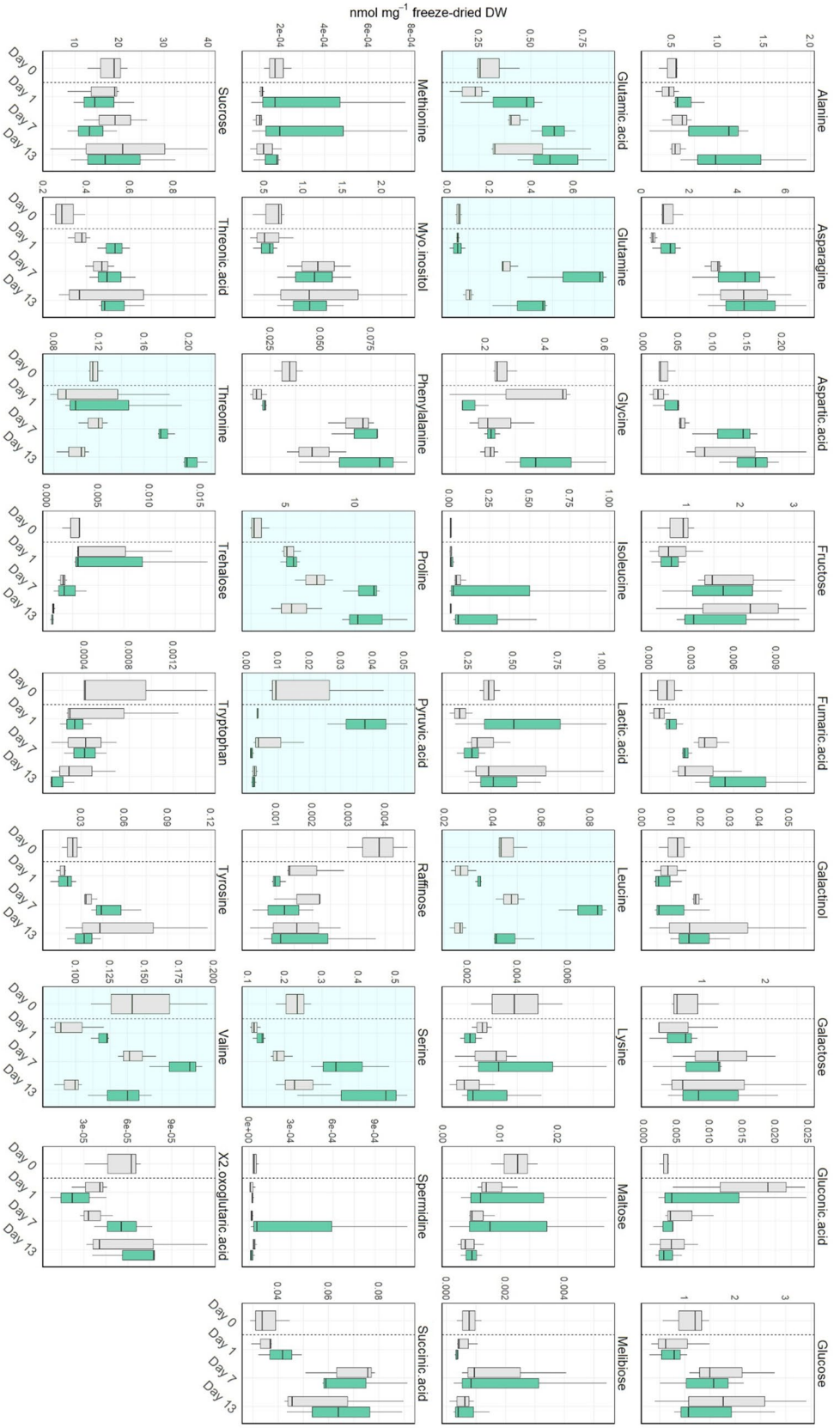

Fig. 8 Absolute quantities of metabolites from GC–MS analysis of *Ulva* tissues. Values are displayed as nmol mg^{-1} DW. The control group is displayed in grey and the ozone treatment group in turquoise. Day 0 samples were collected before the separation of algal material into experimental units and, therefore, represent only one treatment (control) and were not included in statistical testing. Boxes show interquartile ranges (IQR), horizontal lines indicate median values, and whiskers represent the range of the data within 1.5 times the IQR. Metabolites with significant differences identified by repeated measures ANOVA are highlighted with a green background (ozone: n = 3, control: n = 3)

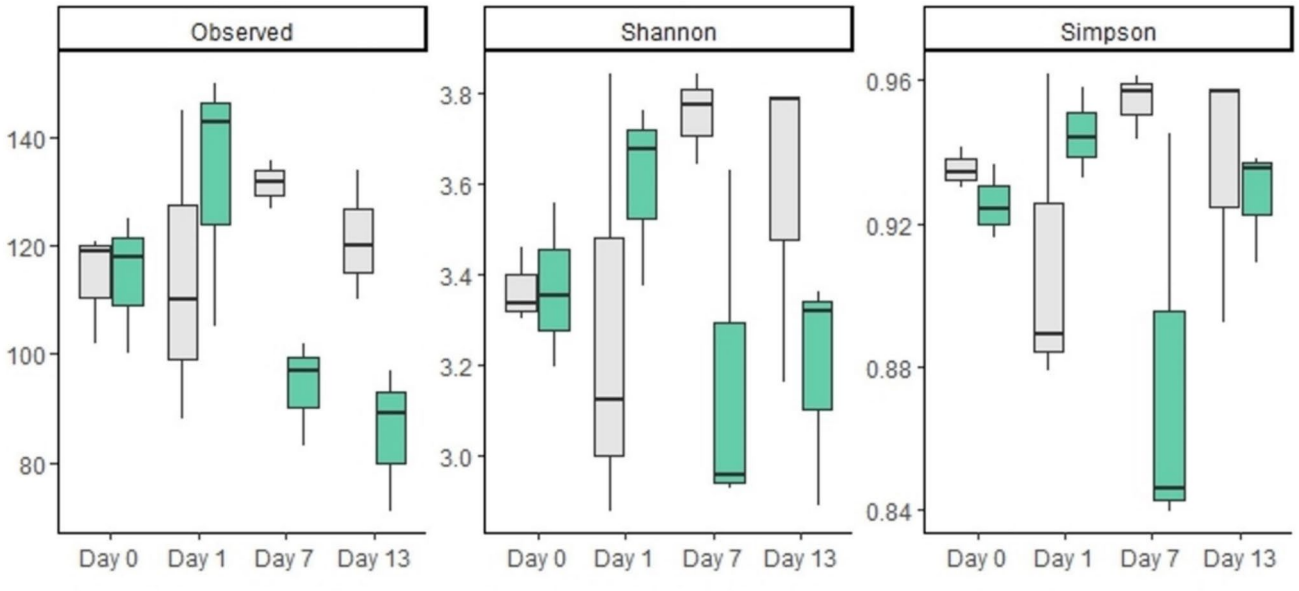

Fig. 9 Alpha Diversity at ASV level: Observed richness, Shannon diversity index, and Simpson diversity index across the duration of the experiment. Diversity metrics were calculated after rarefaction to equal sequencing depth across samples. Observed richness is presented as the number of ASVs, while the Shannon and Simpson indices reflect diversity and evenness within samples. Ozone-treated samples are shown in turquoise and control samples in grey. Boxplots represent interquartile ranges (IQR), with horizontal lines indicating medians and whiskers extending to 1.5 × IQR (control: n = 3, ozone: n = 3)

Phylogenetic characterisation: Ozone vs Control

The most relatively abundant bacterial phyla at the start of the experiment (Day 0) were Proteobacteria (ozone: 47.48 ± 2.07%, control: 42.04 ± 2.62%), Bacteroidota (ozone: 34.02 ± 0.51%, control: 41.26 ± 4.75%), and Actinobacteriota (ozone: 13.44 ± 1.68%, control: 12.90 ± 2.14%). After one day of ozonation, Actinobacteriota sequence abundances increased in the ozone treatment compared to the control (ozone: 14.94 ± 1.51%, control: 10.37 ± 1.98%), whereas Bacteroidota sequence abundances decreased (ozone: 27.41 ± 0.97%, control: 36.21 ± 1.00%). Proteobacteria sequence abundances were similar in both treatments (ozone: 50.44 ± 0.2%, control: 48.20 ± 4.68%).

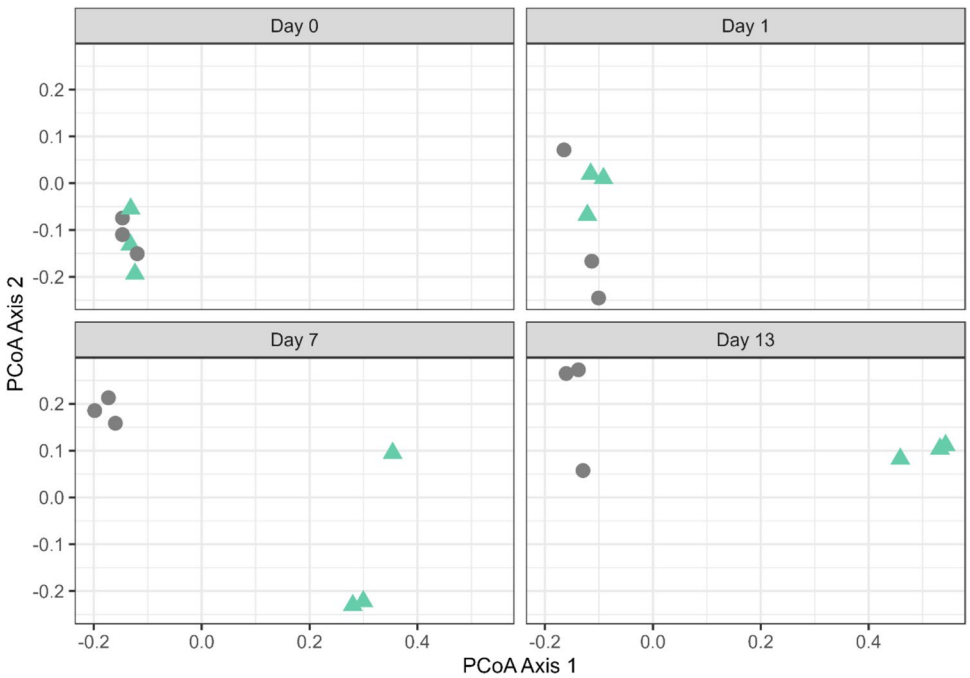

Fig. 10 PCoA of the microbial community associated with *Ulva* tissues. The ordination was calculated from Bray–Curtis dissimilarities between *Ulva* samples based on 16S rRNA gene metabarcoding. Panels are faceted by sampling day (Day 0, 1, 7, 13) to show temporal changes in community composition, but all facets share the same ordination axes. Turquoise triangles represent ozone samples, and grey points represent controls (control: n = 3, ozone: n = 3)

Table 2 PERMANOVA results: 16S rRNA gene metabarcoding data of *Ulva* tissues. The table shows the degrees of freedom (DF), sum of squares (SUMOFSQS), R-squared (R^2), F-statistic (F), and p-value (PR(>F)) for the effects of Day, Treatment, and the interaction between Day and Treatment

	DF	SUMOFSQS	R^2	F	PR(>F)
DAY	3	0.924	0.284	5.422	0.001 ***
TREATMENT	1	0.595	0.183	10.479	0.001 ***
DAY* TREATMENT	3	0.830	0.255	4.869	0.001 ***
RESIDUAL	16	0.909	0.279		
TOTAL	23	3.258	1.000		

By Day 7, ozone exposure led to substantial shifts in sequence abundances: Actinobacteriota decreased to roughly one-third of control values (ozone: 5.63 ± 1.94%, control: 15.37 ± 0.7%) and Bacteroidota to approximately one-fourth (ozone: 9.34 ± 1.56%, control: 39.54 ± 0.93%), while Proteobacteria increased to 83.52 ± 3.49% in the ozone treatment (control: 36.92 ± 1.9%). By Day 13, Actinobacteriota and Bacteroidota sequence abundances remained low in ozone-treated samples (1.03 ± 0.15% and 12.37 ± 1.35%, respectively), compared with controls (13.82 ± 1.84% and 37.64 ± 0.1%), whereas Proteobacteria sequence abundances dominated the ozone treatment (85.99 ± 1.36%) and were less than half of that in controls (40.32 ± 2.51%).

At the family level, Saprospiraceae sequence abundances decreased rapidly in ozone-treated *Ulva*, reaching roughly one-third of control values on Day 1 (ozone: 14.7 ± 1.08%, control: 21.85 ± 0.45%) and continuing to decline through Day 13 (ozone: 0.16 ± 0.02%, control: 26.95 ± 1.43%). Microtrichaceae sequence abundances were initially resilient to ozone (Day 1: ozone: 14.91 ± 1.49%, control: 10.37 ± 1.98%) but declined from Day 7 onward (Day 13: ozone: 1.03 ± 0.15%, control: 13.8 ± 1.82%).

In contrast, some families appeared to benefit from ozonation. Sphingomonadaceae sequence abundances increased from 4.2 ± 0.63% at Day 0 to 14.18 ± 0.32% at Day 13 (control: 0.65 ± 0.07%), and Rhodobacteraceae sequence abundances rose to 24.48 ± 3.25% by Day 13 in ozone-treated *Ulva* (control: 13.88 ± 2.14%). Flavobacteriaceae sequence abundances remained relatively stable, with a notable increase only on Day 13 (ozone: 12.16 ± 1.36%, control: 5.73 ± 0.85%). Methylophilaceae sequence abundances were consistently low in controls (< 1%) but increased under ozone exposure to 5.62 ± 1.82% by Day 13 (Fig. 11).

Differential abundance analysis of microbial ASVs

On Day 1, only 1 ASV (*Colwellia* sp.) exhibited increased abundance. This increase, however, was pronounced, with a 311,000-fold change compared with controls. 5 ASVs (Acidiomicrobiales, 2 *Lewinella*, an OM27_clade bacterium and an uncultured Saprospiraceae) decreased in relative abundances, with ~ 3–507-fold decreases compared with controls (Fig. S2, Supplemental material). After 7 days of ozonation, 15 ASVs (6.5%) increased and 40 (17%) decreased in ozone-treated samples compared with controls. *Pseudophaeobacter* sp. exhibited the highest increase ~ 8,000-fold rise in abundance. *Erythrobacter longus*, *Dokdonia lutea*, *Litorimonas* sp., and *Sphingorhabdus* sp. had also increased in abundance compared with controls. Highly abundant ASVs of *Erythrobacter* sp. (baseMean 373.81), *Methylotenera* sp. (baseMean 344.61), and *Hellea* sp. (baseMean 358.03) — where baseMean represents the mean normalised sequence counts across all samples —had a 6.5—7.5—times abundance increase compared with controls. The top decreasing ASVs were an uncultured bacterium of the Saprospiraceae family (~ 108-fold decrease), *Portibacter lacus* (~ 87-fold decrease), *Planktotalea* sp. (~ 83-fold decrease), and *Yoonia-Loktanella* sp. (~ 80-fold decrease). Notably, an uncultured *Lewinella* and an uncultured bacterium from the Saprospiraceae family showed an almost 100% reduction compared with controls (Fig. S3, Supplemental material).

After 13 days, 25 ASVs (11%) were significantly more abundant, while 46 ASVs (20%) had decreased in abundance compared with controls (Fig. 12). The highest increase was experienced by *Amylibacter* sp. and *Erythrobacter longus* (both ~ 130,000-fold increase), *Kordiimonas* sp., *Dokdonia lutea*, and *Pseudophaeobacter* sp. (~ 5,500–11,500-fold increase). Other high abundance ASVs with significantly 4–16 fold positive changes included *Methylotenera* bacterium WH2-1, *Erythrobacter* sp., *Hellea* sp., and an uncultured bacterium of the KI89A clade. A not well identified bacterium of the Saprospiraceae family experienced the highest negative shift (~ 1,300-fold decrease), followed by *Lewinella* sp. (~ 800-fold decrease). A highly abundant bacterium of the genus *Rubidomonas* had a ~ 30-fold decrease, and another uncultured bacterium of the Saprospiraceae family had a ~ 30-fold decrease. One ASV of the family Microtrichaceae had one of the highest mean abundances (baseMean 519.86) among the significantly changing taxa and showed an ~ 11-fold decline in abundance compared with controls (Fig. 12).

Core microbiomes Ozone vs Control: 13 Days

The core microbiome, here defined as taxa present in at least 20% of samples and with a minimum relative abundance of 2% after log transformation, was dominated by members of the Saprospiraceae family in *Ulva* from the control treatments after 13 days. *Lewinella* sp., *Rubidomonas* sp., and four unidentified Saprospiraceae ASVs together made up 37.5% of all core members (Fig. 13, Table 3). The core

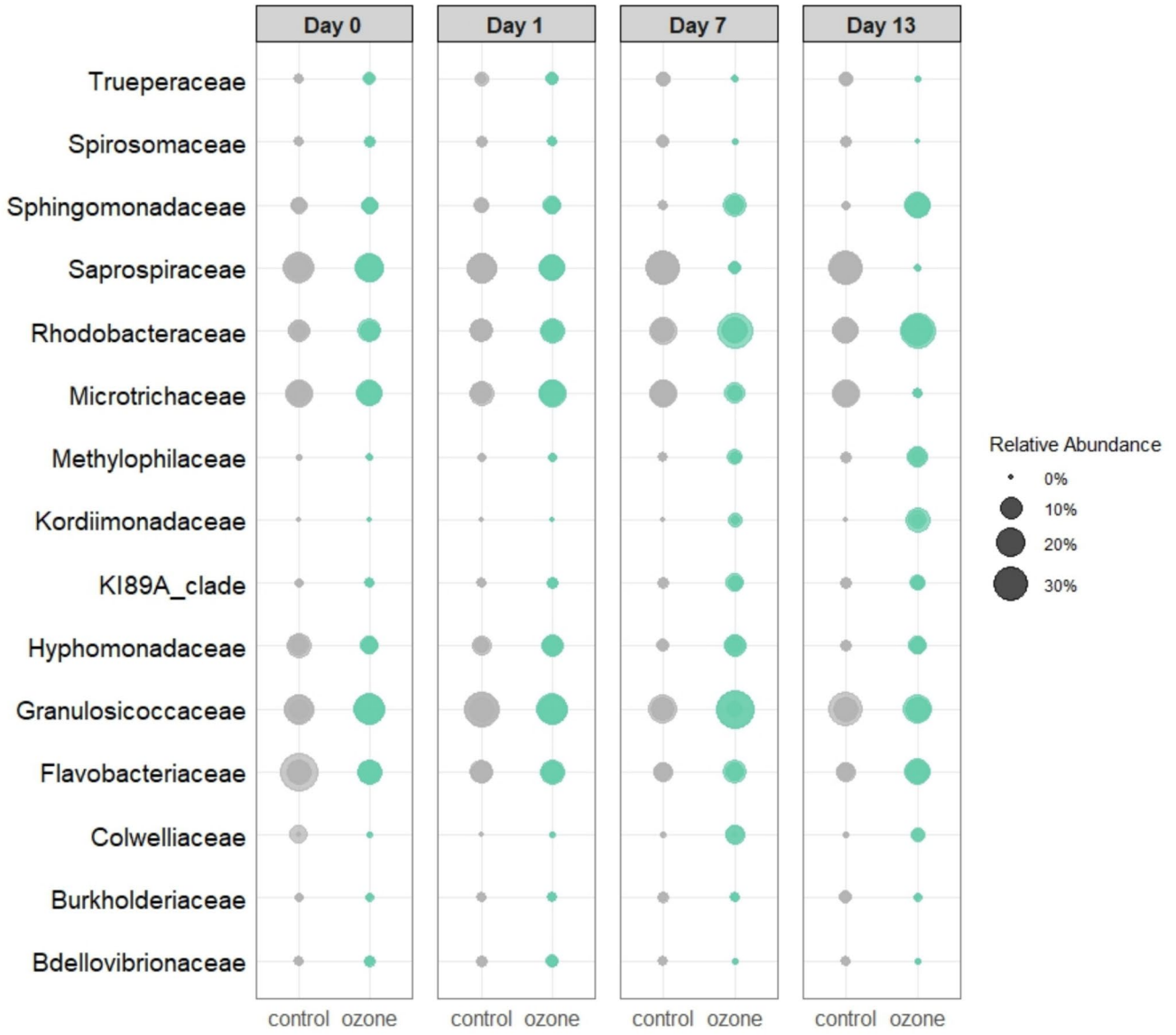

Fig. 11 Bubble plot showing the relative abundances of the 15 most abundant microbial families in ozonated and control *Ulva* microbiomes. Ozone samples are represented in turquoise, and controls in grey (control: n = 3, ozone: n = 3)

also included one unidentified Bacteroidota, three Microtrichaceae, *Maribacter* sp., *Marivita* sp., and *Truepera* sp. Only two ASVs, a *Granulosicococcus* sp., and an uncultured Rhodobacteraceae, were common to both control and ozone treatments. After 13 days of ozonation, the core microbiome of ozonated *Ulva* displayed marked differences at the phylum level, with 87.5% of the microbiome belonging to Proteobacteria and 12.5% to Bacteroidota, compared to controls (52.9% Bacteroidota, 23.53%, Proteobacteria, 17.65% Actinobacteriota, and 5.88% Deinococcota). Many ASVs that were part of the core microbiome in the ozone treatment showed significant increases in differential abundances and relative sequence abundances throughout the experiment, including members of *Amylibacter* sp., *Erythrobacter longus*, *Erythrobacter* sp., *Kordiimonas* sp., *Roseovarius* sp., *Pseudophaeobacter* sp., *Methylotenera* sp., *Sphingorhabdus* sp., and *Dokdonia lutea* (see Fig. 12; Supplemental material, Figs. S5 and S6). The ozonated core microbiome at Day 13 also included *Thalassotalea atypica*, *Aquibacter* sp., and uncultured members of the Rhodobacteraceae, Rhizobiaceae, Hyphomonadaceae, Alteromonadaceae, and the KI89A clade.

Fig. 12 Significant ($p < 0.05$) log2fold changes from DESeq2 differential abundance analysis after 13 days. Log2fold changes are represented as bars, with their corresponding baseMean values displayed. Turquoise bars show ASVs that increased in ozone treatments, while grey bars represent ASVs that declined in ozone treatments compared to controls

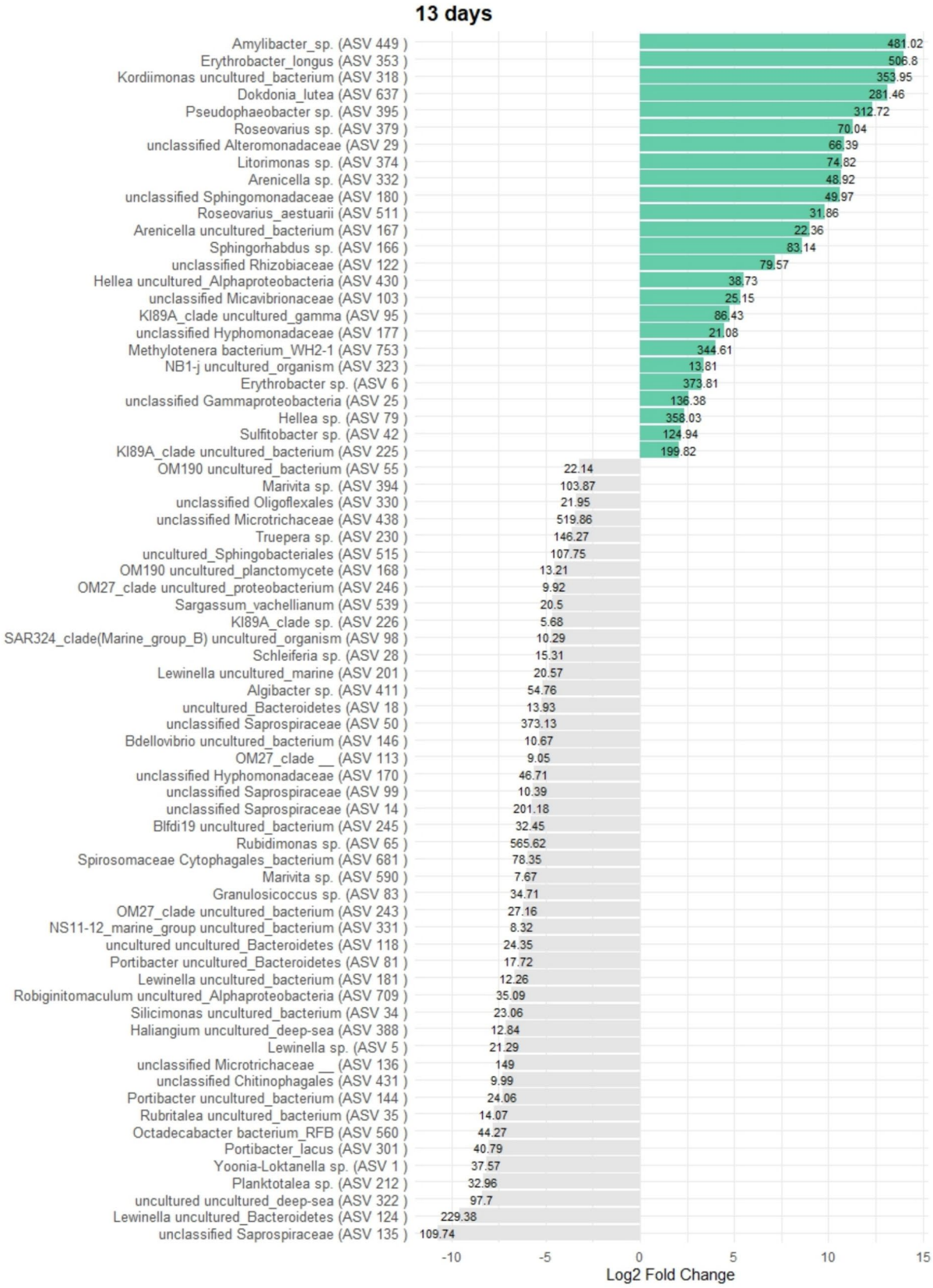
13 days
Amylibacter_sp. (ASV 449)
Erythrobacter_longus (ASV 353)
Kordiimonas uncultured_bacterium (ASV 318)
Dokdonia_lutea (ASV 637)
Pseudophaeobacter sp. (ASV 395)
Roseovarius sp. (ASV 379)
unclassified Alteromonadaceae (ASV 29)
Litorimonas sp. (ASV 374)
Arenicella sp. (ASV 332)
unclassified Sphingomonadaceae (ASV 180)
Roseovarius_aestuarii (ASV 511)
Arenicella uncultured_bacterium (ASV 167)
Sphingorhabdus sp. (ASV 166)
unclassified Rhizobiaceae (ASV 122)
Hellea uncultured_Alphaproteobacteria (ASV 430)
unclassified Micavibrionaceae (ASV 103)
KI89A_clade uncultured_gamma (ASV 95)
unclassified Hyphomonadaceae (ASV 177)
Methylotenera bacterium_WH2-1 (ASV 753)
NB1-j uncultured_organism (ASV 323)
Erythrobacter sp. (ASV 6)
unclassified Gammaproteobacteria (ASV 25)
Hellea sp. (ASV 79)
Sulfitobacter sp. (ASV 42)
KI89A_clade uncultured_bacterium (ASV 225)
OM190 uncultured_bacterium (ASV 55)
Marivita sp. (ASV 394)
unclassified Oligoflexales (ASV 330)
unclassified Microtrichaceae (ASV 438)
Truepera sp. (ASV 230)
uncultured_Sphingobacteriales (ASV 515)
OM190 uncultured_planctomycete (ASV 168)
OM27_clade uncultured_proteobacterium (ASV 246)
Sargassum_vachellianum (ASV 539)
KI89A_clade sp. (ASV 226)
SAR324_clade(Marine_group_B) uncultured_organism (ASV 98)
Schleiferia sp. (ASV 28)
Lewinella uncultured_marine (ASV 201)
Algibacter sp. (ASV 411)
uncultured_Bacteroidetes (ASV 18)
unclassified Saprospiraceae (ASV 50)
Bdellovibrio uncultured_bacterium (ASV 146)
OM27_clade __ (ASV 113)
unclassified Hyphomonadaceae (ASV 170)
unclassified Saprospiraceae (ASV 99)
unclassified Saprospiraceae (ASV 14)
Blfdi19 uncultured_bacterium (ASV 245)
Rubidimonas sp. (ASV 65)
Spirosomaceae Cytophagales_bacterium (ASV 681)
Marivita sp. (ASV 590)
Granulosicoccus sp. (ASV 83)
OM27_clade uncultured_bacterium (ASV 243)
NS11-12_marine_group uncultured_bacterium (ASV 331)
uncultured uncultured_Bacteroidetes (ASV 118)
Portibacter uncultured_Bacteroidetes (ASV 81)
Lewinella uncultured_bacterium (ASV 181)
Robiginitomaculum uncultured_Alphaproteobacteria (ASV 709)
Silicimonas uncultured_bacterium (ASV 34)
Haliangium uncultured_deep-sea (ASV 388)
Lewinella sp. (ASV 5)
unclassified Microtrichaceae __ (ASV 136)
unclassified Chitinophagales (ASV 431)
Portibacter uncultured_bacterium (ASV 144)
Rubritalea uncultured_bacterium (ASV 35)
Octadecabacter bacterium_RFB (ASV 560)
Portibacter_lacus (ASV 301)
Yoonia-Loktanella sp. (ASV 1)
Planktotalea sp. (ASV 212)
uncultured uncultured_deep-sea (ASV 322)
Lewinella uncultured_Bacteroidetes (ASV 124)
unclassified Saprospiraceae (ASV 135)
481.02
506.8
353.95
281.46
312.72
70.04
66.39
74.82
48.92
49.97
31.86
22.36
83.14
79.57
38.73
25.15
86.43
21.08
344.61
13.81
373.81
136.38
358.03
124.94
199.82
22.14
103.87
21.95
519.86
146.27
107.75
13.21
9.92
20.5
5.68
10.29
15.31
20.57
54.76
13.93
373.13
10.67
9.05
46.71
10.39
201.18
32.45
565.62
78.35
7.67
34.71
27.16
8.32
24.35
17.72
12.26
35.09
23.06
12.84
21.29
149
9.99
24.06
14.07
44.27
40.79
37.57
32.96
97.7
229.38
109.74
-10
-5
0
5
10
15
Log2 Fold Change

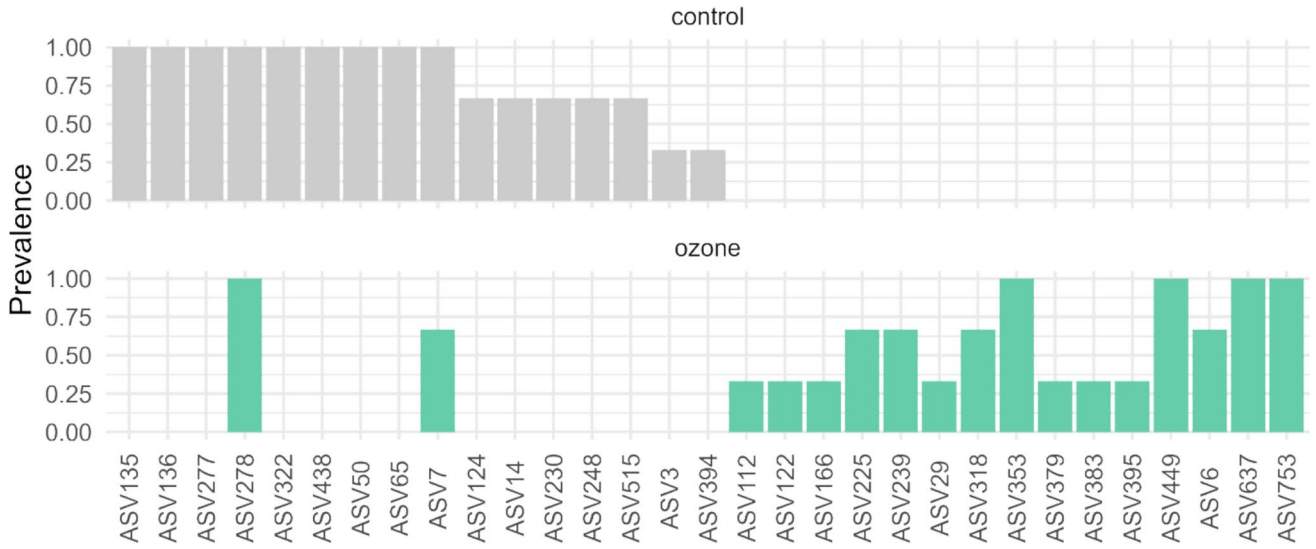

Fig. 13 Core microbiomes of control and ozone samples on Day 13. Shown are the prevalences of microbial ASVs with a relative abundance of 0.02% and 20% sample prevalence. The corresponding taxonomy is shown in Table 3

Discussion

Ulva as a biofilter for ozone-produced oxidants: implications for seaweed cultivation in land-based IMTA systems

In this study, we successfully demonstrated the use of *U. ohnoi* as a biofilter for ozone-produced oxidants (OPO) in a marine IMTA system. Furthermore, we provide first insights into the effects of OPO on a cultivable macroalga, which is particularly relevant for land-based commercial seaweed production. While *Ulva* exhibited signs of stress, which was reflected in reduced biomass gain, altered morphology, and changes in metabolic composition, it maintained considerable growth even at OPO concentrations up to ten times higher than the recommended 'safe concentrations' for sensitive aquaculture species such as turbot (*Psetta maxima*) (Reiser et al. 2010) and Whiteleg shrimp (*Litopenaeus vannamei*) (Schroeder et al. 2010). This tolerance is remarkable, especially given that the redox potentials achieved through ozone injection in this study exceed those typically found in marine environments. Additionally, the observed effects of OPO on *Ulva*-associated microbial biofilms demonstrate ozone's potential to actively shape and manipulate host-associated microbiomes in aquaculture, provided the host species is sufficiently resilient to OPO. These findings position *Ulva* as a promising candidate for integrated water treatment strategies in sustainable aquaculture systems, capable of withstanding oxidative stress while improving water quality.

OPO-lowering capacity of U. ohnoi was consistent, but did not correlate with biomass increase

Our study demonstrated that *U. ohnoi* has potential as a biofilter for ozonation by-products in a marine IMTA system. Mean OPO concentrations in the outflow of *Ulva* cultivation units (0.07 mg L^{-1}) were closer to the 0.06 mg L^{-1} suggested as a 'safe concentration' for some aquaculture species (Reiser et al. 2010; Schroeder et al. 2010) than those measured in the control systems (0.11 mg L^{-1}). This suggests that *Ulva's* presence could provide some protection for *S. aurata* in an IMTA–RAS configuration comparable to that used here. However, the substantial variability in OPO concentrations among replicates represents an important limitation of this study and highlights the need for experiments with a tighter control of inflow OPO concentrations to confirm our results. As we did not directly assess the fate of OPO, it remains unclear whether OPO removal involved direct uptake by *Ulva*, bromide-mediated reactions leading to the formation of brominated compounds within the biomass, or other transformation pathways. However, although *Ulva* species are known to take up bromide for the synthesis of secondary metabolites, this uptake likely occurs via passive diffusion (Paula et al., 1998). Oxidation of bromide by ozone yields more reactive bromine species such as hypobromous acid, hypobromite, and bromamines, which differ in size, charge, and reactivity from bromide and are unlikely to be taken up by *Ulva* in the same way. The observed reduction in OPO concentrations therefore likely results from

Table 3 Core microbiomes of control and ozone samples on Day 13: Corresponding taxonomy (phylum, class, family, genus and species) to ASVs from Fig. 13. Features are colour-coded (control = grey; ozone = turquoise), with bicoloured ASVs represented in both core microbiomes

	ASV	Phylum	Class	Family	Genus	Species
control	ASV135	Bacteroidota	Bacteroidia	Saprospiraceae	_	_
	ASV136	Actinobacteriota	Acidimicrobiia	Microtrichaceae	uncultured	_
	ASV277	Bacteroidota	Bacteroidia	Flavobacteriaceae	*Maribacter*	_
	ASV278	Proteobacteria	Gammaproteobacteria	Granulosicoccaceae	*Granulosicoccus*	uncultured_bacterium
	ASV322	Bacteroidota	Bacteroidia	Saprospiraceae	uncultured	uncultured_deep-sea
	ASV438	Actinobacteriota	Acidimicrobiia	Microtrichaceae	uncultured	uncultured_bacterium
	ASV50	Bacteroidota	Bacteroidia	Saprospiraceae	uncultured	uncultured_bacterium
	ASV65	Bacteroidota	Bacteroidia	Saprospiraceae	*Rubidimonas*	uncultured_bacterium
	ASV7	Proteobacteria	Alphaproteobacteria	Rhodobacteraceae	_	_
	ASV124	Bacteroidota	Bacteroidia	Saprospiraceae	Lewinella	uncultured_Bacteroidetes
	ASV14	Bacteroidota	Bacteroidia	Saprospiraceae	uncultured	_
	ASV230	Deinococcota	Deinococci	Trueperaceae	*Truepera*	uncultured_bacterium
	ASV248	Proteobacteria	Gammaproteobacteria	Burkholderiaceae	*Limnobacter*	uncultured_bacterium
	ASV515	Bacteroidota	Bacteroidia	uncultured	uncultured	uncultured_Sphingobacteriales
	ASV3	Actinobacteriota	Acidimicrobiia	Microtrichaceae	Sva0996_marine_group	_
	ASV394	Proteobacteria	Alphaproteobacteria	Rhodobacteraceae	*Marivita*	_
ozone	ASV112	Proteobacteria	Alphaproteobacteria	Hyphomonadaceae	uncultured	uncultured_bacterium
	ASV122	Proteobacteria	Alphaproteobacteria	Rhizobiaceae	uncultured	uncultured_bacterium
	ASV166	Proteobacteria	Alphaproteobacteria	Sphingomonadaceae	*Sphingorhabdus*	_
	ASV225	Proteobacteria	Gammaproteobacteria	KI89A_clade	KI89A_clade	uncultured_bacterium
	ASV239	Bacteroidota	Bacteroidia	Flavobacteriaceae	*Aquibacter*	_
	ASV29	Proteobacteria	Gammaproteobacteria	Alteromonadaceae	uncultured	uncultured_bacterium
	ASV318	Proteobacteria	Alphaproteobacteria	Kordiimonadaceae	*Kordiimonas*	uncultured_bacterium
	ASV353	Proteobacteria	Alphaproteobacteria	Sphingomonadaceae	*Erythrobacter*	*Erythrobacter_longus*
	ASV379	Proteobacteria	Alphaproteobacteria	Rhodobacteraceae	*Roseovarius*	_
	ASV383	Proteobacteria	Gammaproteobacteria	Colwelliaceae	*Thalassotalea*	*Thalassotalea_atypica*
	ASV395	Proteobacteria	Alphaproteobacteria	Rhodobacteraceae	*Pseudophaeobacter*	_
	ASV449	Proteobacteria	Alphaproteobacteria	Rhodobacteraceae	*Amylibacter*	*Amylibacter*_sp.
	ASV6	Proteobacteria	Alphaproteobacteria	Sphingomonadaceae	*Erythrobacter*	_
	ASV637	Bacteroidota	Bacteroidia	Flavobacteriaceae	*Dokdonia*	*Dokdonia_lutea*
	ASV753	Proteobacteria	Gammaproteobacteria	Methylophilaceae	*Methylotenera*	bacterium_WH2-1

reactions between OPO and organic substrates present in the system, including both seaweed-derived organic matter and reactive components associated with the *Ulva* biomass itself (e.g., surface-bound compounds and biofilms). We did not, however, find a positive correlation between seaweed density and filtering efficiency. This was unexpected, as increased seaweed biomass was anticipated to provide a greater amount of reactive organic substrate capable of reducing OPO. We hypothesise that the OPO produced in our system gradually degraded the exopolymers of the biofilm on *Ulva*, resulting in less organic substrate relative to seaweed biomass available for oxidation by OPO as the experiment progressed. Consequently, the decline in OPO concentrations stagnated despite the growth of *Ulva* biomass. OPO concentrations were measured using the DPD (*N,N*-diethyl-p-phenylenediamine) colorimetric method, which captures overall oxidant activity in the water. Because this approach does not distinguish between individual oxidant species such as aqueous ozone, hypobromous acid, bromamines, or other reactive halogen compounds, the values represent total oxidising capacity rather than specific oxidants. As a result, the exact composition of the oxidants contributing to the measured OPO signal could not be determined, and shifts in individual oxidant species may not be evident from the bulk OPO measurements. Although *Ulva* consistently lowered OPO concentrations in an IMTA system with *S. aurata* in our study, longer experiments are required to confirm this effect and to evaluate the long-term impact on seaweed biomass. Additionally, comparative experiments with other OPO-filtering methods could help contextualise

Ulva's effectiveness relative to more conventional filtration approaches. In wastewater treatment and drinking water pretreatment, methods such as activated carbon filtration and advanced oxidation processes have been shown to effectively reduce concentrations of ozone-related by-products (Chen & Wang 2012; Jiang et al. 2017; MacKeown et al. 2020). However, in aquaculture, and particularly in marine cultivation systems, studies on OPO removability remain scarce. One of the few studies addressing this topic is by Schroeder et al. (2010), which comprehensively evaluated the removal of several types of OPO using activated carbon, with removal efficacies of up to 80% in a lab-based experimental setup. In a case study, Camera-Roda et al. (2019) showed that a combination of photolysis and ozonation ('photocatalytic ozonation') approximately halved bromate formation in a tropical coral reef aquarium and reduced the redox potential in the sump from ~ 600 mV to below 300 mV. Nevertheless, because these studies differ from ours in several key points, such as system design, nutrient loading and OPO measurement methods, direct comparisons of the effectiveness of these approaches are not possible. Addressing this question would require a study design in which OPO removal by *Ulva* and by activated carbon, or by advanced oxidation using an O_3-UV combination, is tested under comparable environmental conditions and for similar exposure times, allowing a meaningful comparison of their effectiveness. Further research on this critical topic of aquaculture water treatment is needed to fully exploit the potential of ozone and related by-product remediation strategies.

Pigments, sugars, and phenolic compounds elevated as a result of oxidative stress exerted by ozone-produced oxidants

Oxidative stress responses in macroalgae often result in a decrease of photosynthetic pigments. The observed increase in total chlorophyll in ozonated *U. ohnoi* was therefore an intriguing find. Pigment elevation as a stress response is not unprecedented. Kakinuma et al. (2006), for example, found an increase in chlorophyll contents and thickened cell walls as a result of organic carbon-redistribution in axenic, temperature-challenged *Ulva pertusa*. They attributed these changes to an adaptive response aimed at maintaining high photosynthesis rates under stressful conditions, which aligns with our findings of slightly decreased photosynthetic efficiency in ozone-stressed *Ulva*. In this context, *U. ohnoi* may have increased pigment production to counterbalance the reduced photosynthetic efficiency caused by oxidative stress. Chlorophyll can function as a potent antioxidant (Cho et al. 2011; Negreanu-Pirjol et al. 2020), and its upregulation in OPO-exposed *Ulva* may reflect an attempt to scavenge reactive oxygen species (ROS). *Ulva rigida* and *Ulva intestinalis* from heavy metal-polluted sites in Morocco exhibited increased cell wall thickness and higher total sugar content than those from control sites (Zeroual et al. 2020). When subjected to UV-B radiation stress, *Ulva prolifera* accumulated starch in its chloroplasts (Zhong et al. 2022), indicating impacts on carbohydrate metabolism as a result of environmental stress. These findings are consistent with the structural changes we observed in ozonated *U. ohnoi* and the elevated soluble carbohydrate concentrations on Day 13, suggesting a similar adaptive response to OPO-induced stress. The antioxidant, antiviral, and antimicrobial properties of phenolic compounds are well established (Lomartire et al. 2021; Bastos et al. 2024), and their elevated levels in *Ulva* subjected to high levels of OPO are therefore not surprising. Phenols, comprising phenolic acids, flavonoids, tannins, stilbenes, coumarins, lignans and lignins in marine algae (Jimenez-Lopez et al. 2021), display protective properties against a wide range of environmental stressors such as metal pollution, herbivory, UV, salinity, and heat stress (Pavia and Brock 2000; Lüder & Clayton 2004; Connan et al. 2007; Cotas et al. 2019; Emeline et al. 2021; Chen et al. 2024). These secondary metabolites are of interest for their potential as food additives and as bioactive agents in pharmaceuticals and cosmetics (Fraga et al. 2019). Our results suggest that ozonation could represent a method for elevating phenolic compound concentrations in commercial production, although in our study, these effects were apparent only after between 7 to 13 days. An increase in ozone dosage might induce a more immediate response, but the effects are likely to vary among algal species and strains.

Metabolomic analysis: GC–MS revealed differential expressions of amino acids involved in proline synthesis

Metabolic profiling of ozonated and control *Ulva* tissues showed that the primary effects of ozonation were on the amino acid compositions. The clearest indicator of environmental stress exerted on *U. ohnoi* by ozonation was the elevated proline content we observed (days 7 and 13). Proline is a well-established marker of oxidative stress in terrestrial plants (Alvarez et al. 2008; Szabados & Savouré, 2010), as well as micro- (Siripornadulsil et al. 2002; Rezayian et al. 2019), and macroalgae (Edwards et al. 1988). Proline's role in stress responses is multifaceted: it functions as an osmolyte, stabilises membranes and redox states, and promotes antioxidant activity (Hong et al. 2000; Siripornadulsil et al. 2002; Rani 2007; Szabados & Savouré, 2010; Ingrisano et al. 2023). In *Ulva*, an increase in proline can be caused by low temperature stress and osmotic changes

(Kakinuma et al. 2006; He et al. 2018). To our knowledge, this is the first study to demonstrate that ozone-produced oxidants can trigger this molecular stress response in *U. ohnoi*. The enhanced concentrations of glutamine and glutamic acid after 7 and 13 days of ozonation further support this observation, as these amino acids are key intermediates in the proline biosynthesis pathway (Fichman et al. 2015; He et al. 2018).

Alanine, leucine, and valine, which are all products of the same biosynthetic pathway, were significantly elevated in ozone-treated *Ulva* tissues. As all three amino acids are derived from pyruvate, the end product of glycolysis, this may be linked to the peak in pyruvic acid (the protonated form of pyruvate) observed on Day 1, potentially reflecting a temporary metabolic bottleneck. An interpretation of their elevated levels is not as straightforward as with proline, but some of these amino acids have been reported to be differentially expressed in response to stress in *Chlorella* spp. (Shakya et al. 2022), *Ectocarpus siliculosus* (Dittami et al. 2011), and *Skeletonema marinoi* (Nikitashina et al. 2022). He et al. (2018) observed that high-temperature stress in *U. prolifera* altered the alanine/aspartate/glutamate metabolic pathways, leading to increased levels of alanine, serine, valine, and leucine. Threonine, which was significantly elevated in ozonated *U. ohnoi* on Day 7 and 13, serves as a precursor for branched-chain amino acids (BCAAs) such as valine and isoleucine. BCAAs are implicated in abiotic stress responses in plants, for instance by functioning as osmolytes (Joshi et al. 2010). Additionally, a trend towards elevated phenylalanine levels in ozonated *Ulva* on Days 7 and 13 may be linked to the concurrent observed increases in phenols, flavonoids, and tannins, as phenylalanine and tyrosine are key precursors in the biosynthesis of these stress-associated secondary metabolites (Kumari et al. 2023).

No significant differences between treatments were observed in any of the mono- and disaccharides detected by GC–MS, suggesting that the elevated soluble sugar levels measured in ozonated *U. ohnoi* were likely due to polysaccharides. Ulvan, a soluble polysaccharide responsible for maintaining cell wall stability, occurs in significant amounts in members of the Ulvaceae (Dominguez & Loret 2019; Sari-Chmayssem et al. 2019). An upregulation of ulvan biosynthesis in response to OPO exposure could explain the observed increase in ozonated *Ulva* rigidity. Because the metabolite analysis was restricted to a targeted set of primarily low-molecular-weight compounds, potential changes in high-molecular-weight metabolites such as ulvan could not be directly assessed. As this compound is of considerable commercial interest (Cunha & Grenha 2016; Hosseini et al. 2024), future studies on the impacts of ozonation on *Ulva* should consider the role of ulvan in its response to high OPO concentrations and apply appropriate methods to detect them.

Nutrient availability and biofilm restructuring under OPO-rich conditions shape U. ohnoi microbiome

Temporal fluctuations in microbial communities in seaweeds are well-documented (Nguyen et al. 2023; van der Loos et al. 2024a, b), so the effect of time on community composition even in our control samples was expected. After 13 days, the core microbiome in control samples consisted of 17 ASVs from the phyla Bacteroidota, Proteobacteria, Actinobacteria, and Deinococcota. In contrast, the core microbiome in ozone-treated samples comprised 15 ASVs, with 14 belonging to the class Alphaproteobacteria and only one to Bacteroidota. Proteobacteria, Bacteroidota, and Actinobacteria are commonly associated with seaweeds like *Ulva* (Bolton et al. 2016; Steinhagen et al. 2021). The decline in diversity at the phylum level was partly reflected in the alpha diversity measures at the ASV level, although the effects were less pronounced than anticipated. The strongest effects of ozonation were evident in the declining observed richness at Days 7 and 13. Additionally, DESeq2 analysis revealed that there was a higher number of declining ASVs than increasing ones at all sampling days. Although no statistically significant differences were detected in either alpha diversity metric at any time point, this likely reflects limited statistical power due to the small sample size rather than an absence of an effect. The negative trend in microbial diversity observed in the ozone treatments suggests a general decrease in diversity in *U. ohnoi*–associated communities, which may become more pronounced with prolonged exposure. The lack of strong short-term responses, however, suggests that the microbial community may exhibit some resilience to brief ozone exposure.

The control core microbiome shared similarities with *Ulva*-associated communities reported across diverse environments, including natural marine habitats, land-based cultivation, and IMTA systems, where Flavobacteriaceae, Saprospiraceae, Rhodobacteraceae, Microtrichaceae and Hyphomonadaceae, and genera such a *Lewinella*, *Maribacter*, and *Granulosicoccus* are often dominant (Burke et al. 2011; Califano et al. 2020; Nguyen et al. 2023; van der Loos et al. 2023, 2024a, b; Peña-Rodríguez et al. 2024). The core microbiomes in our ozone treatment, on the other hand, harboured the genera *Dokdonia, Erythrobacter* and *Methylotenera*, as well as members of Hyphomonadaceae, Flavobacteraceae, Sphingomonadaceae and Rhodobacteraceae families. While some (like *Dokdonia* and *Erythrobacter*) have been found in association with *Ulva* before, other genera that thrived under ozonation are not typically associated with *Ulva* microbiomes. *Kordiimonas* sp., a genus usually underrepresented in Ulvaceae communities, became a highly abundant core member in ozonated *U. ohnoi*, suggesting an opportunistic advantage. Similarly, *Methylotenera*, which

are not commonly considered *Ulva* symbionts, emerged as core community members under ozonation. The reasons for the emergence of this genus in the ozone treatment will be discussed further.

One of the most noteworthy observations regarding the effects of OPO on the *Ulva* microbiome was the gradual disappearance of bacteria specialised in degrading complex carbohydrates. We attribute this observation to the properties of OPO, which reportedly degrade a wide range of natural and manmade molecules in aquaculture (Summerfelt 2003; Phungsai et al. 2019; Aguilar-Alarcón et al. 2022; Pettersson et al. 2022). Bacteroidota experienced the most significant reductions in abundance, likely due to the disappearance of complex carbohydrates from the phycosphere, for which these bacteria are recognised as key degraders (McKee et al. 2021). Members of the family Saprospiraceae, including *Lewinella*, *Rubidomonas*, and *Portibacter*, were most affected by ozone treatments. Saprospiraceae have been found associated with *Ulva* in IMTA settings (Califano et al. 2020), and genomic data reveal their capacity to degrade complex carbohydrates like starch, gelatin, and alginate (McIlroy & Nielsen 2014). In contrast, *Amylibacter*, *Kordiimonas*, and *Erythrobacter* (all Alphaproteobacteria), which experienced increased relative abundances under ozone conditions, show genomic potential for metabolising low-molecular-weight carbohydrates such as monosaccharides, peptides, and esters (Koblízek et al. 2011; Tonon et al. 2014; Nedashkovskaya et al. 2016; Geng et al. 2022; Ye et al. 2022). *Dokdonia lutea*, one of the few ozone-enriched Bacteroidota members, lacks polysaccharide lyases but possesses several esterase-encoding genes, suggesting a preference for short-chain esters over complex carbohydrates (González et al. 2011). Based on these findings, we conclude that one of the main ways in which OPO shaped the *Ulva* microbiome is through the degradation of complex carbohydrates contained in the biofilm.

While -omics techniques have significantly advanced our understanding of the composition and functional potential of algae-associated microbial communities, relatively little is known about the spatial distribution of individual epibiont taxa within bacterial biofilms. Ramírez-Puebla et al. (2022) provided a rare glimpse into this spatial organisation by applying fluorescence in-situ hybridisation (FISH) to biofilms on *Nereocystis luetkeana*, revealing a layered structure with *Granulosicoccus* cells clustered near the kelp surface and filamentous Alphaproteobacteria and Bacteroidota positioned close to the seawater-biofilm interface. In our study, one *Granulosicoccus* sp. was consistently associated with *Ulva* in both ozone and control treatments, suggesting a potentially symbiotic relationship. Proximity plays a crucial role in both microbe-microbe and host-microbe interactions, particularly in high-flow environments (Cordero & Datta 2016; Co et al. 2020). *Granulosicoccus'* positioning near the algal surface may therefore facilitate close interaction with the host and simultaneously confer protection against OPO-mediated biofilm degradation. Members of this genus are known to degrade algal-derived complex carbohydrates such as alginate, and possess a complete set of BCha genes, enabling photoheterotrophic growth (Weigel et al. 2022). This metabolic flexibility, in combination with favourable spatial localisation, may explain the persistence of *Granulosicoccus* in *Ulva*-associated biofilms under ozonation. Ramírez-Puebla et al. (2022) also reported the presence of Bacteroidota within the intercellular spaces of kelp tissues, suggesting that some ASVs enriched under ozonation in our study may represent bacterial endosymbionts. If so, their location within *Ulva* tissue could have shielded them from the oxidative degradation of the external biofilm matrix.

Host–microbe metabolic coupling and stress resilience

The observed shifts in the microbial community associated with *U. ohnoi* under ozone treatment suggest that bacteria in close association with the host, and in particular those specialised in utilising *Ulva*-derived dissolved organic matter (DOM), are more likely to persist under oxidative stress. Under controlled conditions, epibiotic bacteria can degrade and metabolise both *Ulva*-derived and bacterial exopolysaccharides. However, when the biofilm is compromised, bacterial persistence within the phycosphere appears to depend more on the direct provision of photosynthates by the host than on the breakdown of complex algal exudates or microbial exopolymers. This could also explain the pronounced increase in *Roseovarius'* relative abundance under ozonation, which is a known growth-promoting symbiont of *Ulva* that metabolises glycerol provided by the alga (Alsufyani et al. 2017). Certain strains of *Roseovarius* also display strong reactive oxygen species (ROS)-scavenging potential (Heric et al. 2023), which could provide an advantage to *Ulva* under OPO-enriched conditions. The genera *Roseovarius*, *Sulfitobacter* and *Maribacter* are moreover known to harbour species that produce AGMPFs (algal growth and morphogenesis-promoting factors), molecular compounds essential for *Ulva* growth and development (Ghaderiardakani et al. 2017; Alsufyani et al. 2020). Previous research has shown that they remain consistently in the microbiome of *U. compressa* under micropollutant stress (Hardegen et al. 2025), and some strains may even confer protection against environmental stressors such as high temperature (Hmani et al. 2024). The fact that *Roseovarius* and *Sulfitobacter* increased in relative abundance under ozone treatment and *Maribacter* was not negatively affected (Supplemental Fig. S5) align with the work of Hardegen et al. (2025) and support the notion that functional members of the *Ulva* microbiome are rather resilient towards environmental stress

as experienced in various bioremediation setups. Seaweed microbiomes may play a protective role under stressful environmental conditions. and *Ulva* could actively promote the growth of symbionts that confer these protective functions, an idea consistent with Hylleberg's concept of microbial gardening (Hylleberg 1975).

Roseovarius is also among the *Ulva* symbionts capable of sensing DMSP, a molecule secreted by seaweeds that can induce chemotaxis in marine microbes (Kessler et al. 2018). DMSP serves multiple functions, including acting as a cryoprotectant (Kirst et al. 1991; Toda et al. 2023), fouling-deterrent (Saha et al. 2012), osmoprotectant (Lyon et al. 2016), and antioxidant (Sunda et al. 2002). Stressed seaweeds excrete higher amounts of DMSP (Sunda et al. 2002), potentially attracting more symbionts with the ability to either sense or metabolise it. Elevated DMSP concentrations have, for example, been shown to favour the growth of Rhodobacteraceae and Flavobacteriaceae under temperature and light stress in *Fucus*, while inhibiting the growth of *Firmicutes* (Saha et al. 2014). Ozonation and high OPO concentrations likely represent a physiological stressor that may lead to increased excretion of DMSP. *Roseovarius,* which highly increased in ozone treatments, does not use DMSP as a carbon source, but cleaves it into dimethylsulphide and methanethiol (Kessler et al. 2018), likely providing a substrate for *Methylotenera*. Members of this genus exclusively use methanol and methylamines as a carbon source (Afshin et al. 2021), and their abundance was significantly increased in ozonated *Ulva* compared with controls. After 13 days of ozonation, *Methylotenera* bacterium WH2-1 even constituted a part of the core microbiome. Other ozone-enriched genera, which are suspected to metabolise DMSP via the demethylation pathway or the cleavage pathway, are *Sulfitobacter* (Curson et al. 2008; Zeng et al. 2020; Xu et al. 2024), *Pseudophaeobacter* (Liu et al. 2023), and *Amylibacter* (O'Brien et al. 2022).

Because ozone oxidises ammonia to nitrate, we anticipated that the ability to utilise nitrate as a nitrogen source could additionally influence microbial community structure in ozonated *Ulva*. Potential for nitrate reduction or assimilation has been reported for several genera enriched under ozonation, including *Roseovarius*, *Arenicella*, *Granulosicoccus*, *Kordiimonas, Litorimonas, Hellea* and *Methylotenera* (Abraham & Rohde 2014; Kits et al. 2015; Kang et al. 2018; Castro et al. 2020; Afshin et al. 2021; van Grinsven et al. 2021; Slobodkina et al. 2022; Weigel et al. 2022; Ye et al. 2022), as well as in *Erythrobacter longus* (Tonon et al. 2014). In contrast, members of the family Saprospiraceae, which thrive in ammonia-rich environments (Kondrotaite et al. 2022), generally lack the capacity for nitrate reduction (McIlroy & Nielsen 2014; Weigel et al. 2022). Their decline under ozonation could therefore be due to nitrogen limitation. *Portibacter lacus*, which declined sharply under ozonation, was also found unable to reduce nitrate (Yoon et al. 2012). Future studies on the effects of ozonation in seaweed cultivation should include nutrient measurements to better link microbiome changes to nutrient availability.

Cobalamin synthesis, catalase and oxidase activity, and osmolytes: potential advantages for microbial symbionts under elevated OPO-concentrations

Several other factors could have contributed to the observed shifts in ozone-exposed microbiomes. We observed a relative increase in ASVs with a reported genetic potential of synthesising cobalamin (B12) in OPO-exposed *Ulva,* including *Amylibacter* (Nedashkovskaya et al. 2016), *Granulosicoccus* (Weigel et al. 2022), *Kordiimonas* (Ye et al. 2022), *Arenicella* (Weigel et al. 2022), *Erythrobacter* (Koblízek et al. 2011), and *Pseudophaeobacter* (Zhu et al. 2023). In ozone-sensitive Saprospiraceae, on the other hand, metagenomic shotgun sequencing has revealed a general lack of Cobalamin-synthesis genes (Wang et al. 2022). Cobalamin is a scarce resource in marine environments but confers enhanced resistance to various environmental stressors in bacteria (Ferrer et al. 2016; Mars Brisbin et al. 2023). Most seaweeds cannot synthesise it and must rely on their microbial symbionts for its provision (Croft et al. 2005). It is therefore likely that stressed seaweeds with increased metabolic activity due to environmental stress (e.g., ozonation) may enhance their selection for B12-producing bacteria. However, not all cobalamin producers export the compound, and it therefore remains unclear whether these taxa directly contribute to host nutrition or primarily benefit from their own enhanced stress tolerance. Other factors, such as catalase and oxidase, may confer resistance to ROS generated in OPO-rich environments (Giuffrè et al. 2014; Yuan et al. 2021). Presence of these enzymes has been confirmed in ozone-resistant genera *Sulfitobacter*, *Hellea*, *Sphingorhabdus*, and *Methylotenera* (Kalyuzhnaya et al. 2006; Alain et al. 2008; Jogler et al. 2013; Glaeser & Kämpfer 2014; Jung et al. 2019; Afshin et al. 2021; Xu et al. 2024). Additional features imbuing resistance could be the expression of osmoregulators such as ectoine, proline, the proline-derivative betaine, and hemerythrin-binding proteins (genetic potential described for example for *Pseudophaeobacter arcticus*).

Identifying bacterial traits that confer resistance to ozone treatments in the *Ulva* microbiome could help predict the potential of ozonation as a strategy for controlling specific pathogens in aquaculture. Many diseases in algae aquaculture such as 'ice-ice' (Largo et al. 1995) and bleach disease (Liu et al. 2019) are caused by Bacteroidota, and members of the phylum have been identified as a health threat to many marine organisms (Hudson & Egan 2022). In our

study, Bacteroidota were significantly impacted by ozone treatment, suggesting that ozonation could potentially be used to combat these diseases in aquaculture. However, the sensitivity of the host to ozone-treated water (OPO) must be carefully considered. While tolerance thresholds for many aquaculture organisms remain poorly understood, this study is the first to explore the effects of OPO on a macroalga. Our results show that *U. ohnoi* was able to withstand and adapt to high levels of OPO, a condition that would likely be harmful to many fish and crustaceans in aquaculture, yet further research is needed to investigate the effects of ozonation on other commonly cultivated algal genera and their associated microbiomes.

Conclusions

We conclude that *U. ohnoi* can effectively mitigate toxic ozonation by-products in marine Integrated Multi-Trophic Aquaculture (IMTA) systems. However, ozonation-induced degradation of *Ulva* biofilms will likely reduce OPO-lowering efficiency over time, as the ratio of available substrate for OPO oxidation decreases relative to biomass. Additionally, exposure to OPO may alter *Ulva*'s metabolic composition by triggering an oxidative stress response, suggesting that ozone could serve as a tool to actively modify *Ulva* biomass quality. OPO exposure also impacts microbial communities within *Ulva* biofilms, probably both by physically restructuring the phycosphere through exo-polysaccharide degradation and by influencing nutrient availability. Growth-promoting bacteria releasing AGMPFs are present even under high OPO conditions. These findings provide valuable insights into how ozonation shapes aquaculture microbiomes and its potential role in aquaculture management.

Supplementary Information The online version contains supplementary material available at https://doi.org/10.1007/s10811-026-03850-8.

Acknowledgements We would like to thank the Estação Piloto de Piscicultura de Olhão (EPPO) for the provision of *Ulva* biomass. We also wish to thank António Vieira for the provision of space, resources, and consultancy, João Cruz for technical support during the experimental phase, and Dr. Sabine Keuter for technical support and the pre-processing of 16S rRNA metabarcoding data. We wish to thank Constanze von Waldthausen for support with laboratory analyses, Matthias Birkicht for his contributions to OPO measurements, and Brittany Beaudry for conducting DNA barcoding of the *Ulva* specimens used in this study. Microbiome sequencing received infrastructure support from the DFG Research Unit 5042 "miTarget" and the DFG Excellence Cluster 2167 "Precision Medicine in Chronic Inflammation" (PMI).

Author contribution SW: Conceptualisation (lead); methodology (lead); investigation (lead); data curation (lead); formal analysis (lead); writing – original draft (lead). CP: investigation (equal); formal analysis (equal); writing – review and editing (equal). TA: review and editing (equal). AE: supervision (equal); resources (equal); writing – review and editing (lead). MB: formal analysis (supporting); review and editing (equal); WW: resources (equal); review and editing (equal); AK: supervision (lead); resources (equal); writing – review and editing (equal); funding acquisition (lead).

Funding Open Access funding enabled and organized by Projekt DEAL. SW and AK received funds from AiF Projekt GmbH (FKZ KK5393101AD1). This study received Portuguese national funds from FCT—Foundation for Science and Technology—through projects UIDB/04326/2020, UIDP/04326/2020, and contract CEECINST/00114/2018 to AE.

Data availability Data supporting the findings of this study are available within the paper and its Supplementary Information. All sequencing data were deposited at the NCBI Sequence Read Archive (SRA) under the accession number PRJNA1356848.

Declarations

Use of AI Statement During the preparation of this work the author(s) used ChatGPT (OpenAI) to improve language and clarity in certain sections. After using this tool, the authors reviewed and edited the content as needed and take full responsibility for the content of the publication.

Competing interests The authors declare no competing interests.

References

Abraham WR, Rohde M (2014) The family Hyphomonadaceae. In: Rosenberg E, DeLong EF, Lory S, Stackebrandt E, Thompson F (eds) The Prokayotes. Alphaproteobacteria and BetaProteobacteria. 4th Edn. Springer, Heidelberg, pp 283–299

Afshin Y, Delherbe N, Kalyuzhnaya MG (2021) *Methylotenera*. In: Trujillo ME, Dedysh S, DeVos P, Hedlund B, Kämpfer P, Rainey FA, Whitman WA (eds) Bergey's Manual of Systematics of Archaea and Bacteria, Wiley, pp 1–11

Aguilar-Alarcón P, Zherebker A, Rubekina A, Shirshin E, Simonsen MA, Kolarevic J, Lazado CC, Nikolaev EN, Asimakopoulos AG, Mikkelsen Ø (2022) Impact of ozone treatment on dissolved organic matter in land-based recirculating aquaculture systems studied by Fourier transform ion cyclotron resonance mass spectrometry. Sci Total Environ 843:157009

Alain K, Tindall BJ, Intertaglia L, Catala P, Lebaron P (2008) *Hellea balneolensis* gen. nov., sp. nov., a prosthecate alphaproteobacterium from the Mediterranean Sea. Int J Syst Evol Microbiol 58:2511–2519

Alsufyani T, Weiss A, Wichard T (2017) Time course exo-metabolomic profiling in the green marine macroalga *Ulva* (Chlorophyta) for identification of growth phase-dependent biomarkers. Mar Drugs 15:14

Alsufyani T, Califano G, Deicke M, Grueneberg J, Weiss A, Engelen AH, Kwantes M, Mohr JF, Ulrich JF, Wichard T (2020) Macroalgal–bacterial interactions: identification and role of thallusin in morphogenesis of the seaweed *Ulva* (Chlorophyta). J Exp Bot 71:3340–3349

Alvarez S, Marsh EL, Schroeder SG, Schachtman DP (2008) Metabolomic and proteomic changes in the xylem sap of maize under drought. Plant Cell Environ 31:325–340

Angell AR, Mata L, de Nys R, Paul NA (2015) Indirect and direct effects of salinity on the quantity and quality of total amino acids in *Ulva ohnoi* (Chlorophyta). J Phycol 51:536–545

Barzkar N, Jahromi ST, Poorsaheli HB, Vianello F (2019) Metabolites from marine microorganisms, micro, and macroalgae: immense scope for pharmacology. Mar Drugs 17:464

Bastos CFS, Carpena M, Chamorro F, Nogueira-Marques R, Silva A, Barroso MF, Santos M, Prieto MA (2024) Phlorotannins as bioactive agents from brown algae: chemical characterization and extraction methods. Proceedings 103(1):61

Bates D, Mächler M, Bolker B, Walker S (2015) Fitting linear mixed-effects models using lme4. J Stat Softw 67:1–48

Batır E, Metin Ö, Yıldız M, Özel OT, Fidan D (2024) Sustainable land-based IMTA: holistic management of finfish, mussel, and macroalgae interactions, emphasizing water quality and nutrient dynamics. J Environ Manage 372:123411

Biju J, Sulaiman CT, Sateesh G, Reddy VRK (2014) Total phenolics and flavonoids in selected medicinal plants in Kerala. Int J Pharm Pharm Sci 6:406–408.

Bokulich NA, Kaehler BD, Rideout JR, Dillon M, Bolyen E, Knight R, Huttley GA, Caporaso GJ (2018) Optimizing taxonomic classification of marker-gene amplicon sequences with QIIME 2's q2-feature-classifier plugin. Microbiome 6:90

Bolton JJ, Cyrus MD, Brand MJ, Joubert M, Macey BM (2016) Why grow *Ulva*? Its potential role in the future of aquaculture. Perspect Phycol 3:113–120

Bolyen E, Rideout JR, Dillon MR, Bokulich NA, Abnet CC et al (2019) Reproducible, interactive, scalable and extensible microbiome data science using QIIME 2. Nat Biotechnol 37:852–857

Broadhurst RB, Jones WT (1978) Analysis of condensed tannins using acidified vanillin. J Sci Food Agric 29:788–794

Bruhn A, Dahl J, Nielsen HB, Nikolaisen L, Rasmussen MB, Markager S, Olesen B, Arias C, Jensen PD (2011) Bioenergy potential of *Ulva lactuca:* biomass yield, methane production and combustion. Bioresour Technol 102:2595–2604

Burke C, Thomas T, Lewis M, Steinberg P, Kjelleberg S (2011) Composition, uniqueness and variability of the epiphytic bacterial community of the green alga *Ulva australis*. ISME J 5:590–600

Calheiros AC, Reis RP, Castelar B, Cavalcanti DN, Teixeira VL (2019) *Ulva* spp. as a natural source of phenylalanine and tryptophan to be used as anxiolytics in fish farming. Aquaculture 509:171–177

Calheiros AC, Sales LPM, Pereira Netto AD, Cavalcanti DN, Castelar B, Reis RP (2021) Commercial raw materials from algaculture and natural stocks of *Ulva* spp. J Appl Phycol 33:1805–1818

Califano G, Kwantes M, Abreu MH, Costa R, Wichard T (2020) Cultivating the macroalgal holobiont: effects of Integrated Multi-Trophic Aquaculture on the microbiome of *Ulva rigida* (Chlorophyta). Front Mar Sci 7: 52

Callahan BJ, McMurdie PJ, Rosen MJ, Han AW, Johnson AJA, Holmes SP (2016) DADA2: high-resolution sample inference from Illumina amplicon data. Nat Methods 13:581–583

Camera-Roda G, Loddo V, Palmisano L, Parrino F (2019) Photocatalytic ozonation for a sustainable aquaculture: a long-term test in a seawater aquarium. Appl Catal B 253:69–76

Caporaso JG, Lauber CL, Walters WA, Berg-Lyons D, Huntley J, Fierer N, Owens SM, Betley J, Fraser L, Bauer M, Gormley N, Gilbert JA, Smith G, Knight R (2012) Ultra-high-throughput microbial community analysis on the Illumina HiSeq and MiSeq platforms. ISME J 6:1621–1624

Castro DJ, Gomez-Altuve A, Reina JC, Rodríguez M, Sampedro I, Llamas I, Martínez-Checa F (2020) *Roseovarius bejariae* sp. nov., a moderately halophilic bacterium isolated from a hypersaline steep-sided river bed. Int J Syst Evol Microbiol 70:3194–3201

Cesare Marincola F, Palmas C, Lastres Couto MA, Paz I, Cremades J, Pintado J, Bruni L, Picone G (2025) Metabolic profile of Senegalese sole (*Solea senegalensis*) muscle: effect of fish–macroalgae IMTA-RAS aquaculture. Molecules 30:2518

Chang CC, Yang MH, Wen HM, Chern JC (2002) Estimation of total flavonoid content in propolis by two complementary colometric methods. J Food Drug Anal 10:178–182

Chatzoglou E, Kechagia P, Tsopelakos A, Miliou H, Slembrouck J (2020) Co-culture of *Ulva* sp. and *Dicentrarchus labrax* in recirculating aquaculture system: effects on growth, retention of nutrients and fatty acid profile. Aquac Living Resour 33:19

Chen X, Tang Y, Zhang H, Zhang X, Sun X, Zang X, Xu N (2024) Physiological, transcriptome, and metabolome analyses reveal the tolerance to Cu toxicity in red macroalgae *Gracilariopsis lemaneiformis*. Int J Mol Sci 25:4770

Chen K-C, Wang Y-H (2012) Control of disinfection by-product formation using ozone-based advanced oxidation processes. Environ Technol 33:487–495

Cho M, Lee HS, Kang IJ, Won MH, You S (2011) Antioxidant properties of extract and fractions from *Enteromorpha prolifera*, a type of green seaweed. Food Chem 127:999–1006

Chopin T, Buschmann AH, Halling C, Troell M, Kautsky N, Neori A, Kraemer GP, Zertuche-González JA, Yarish C, Neefus C (2001) Integrating seaweeds into marine aquaculture systems: a key toward sustainability. J Phycol 37:975–986

Chopin T, Robinson SMC, Troell M, Neori A, Buschmann AH, Fang J (2008) Multitrophic integration for sustainable marine aquaculture. In: Jorgensen SE, Fath BD (eds) The Encycopedia of Ecology. Vol 3. Ecological Engineering. Elsevier, Oxford, pp 2463–2475

Chopin T, Tacon AGJ (2021) Importance of seaweeds and extractive species in global aquaculture production. Rev Fish Sci Aquac 29:139–148

Co AD, van Vliet S, Kiviet DJ, Schlegel S, Ackermann M (2020) Short-range interactions govern the dynamics and functions of microbial communities. Nature Ecol Evol 4:366–375

Connan S, Deslandes E, Gall EA (2007) Influence of day–night and tidal cycles on phenol content and antioxidant capacity in three temperate intertidal brown seaweeds. J Exp Mar Biol Ecol 349:359–369

Cordero OX, Datta MS (2016) Microbial interactions and community assembly at microscales. Curr Opin Microbiol 31:227–234

Cotas J, Figueirinha A, Pereira L, Batista T (2019) The effect of salinity on *Fucus ceranoides* (Ochrophyta, Phaeophyceae) in the Mondego river (Portugal). J Oceanol Limnol 37:881–891

Croft MT, Lawrence AD, Raux-Deery E, Warren MJ, Smith AG (2005) Algae acquire vitamin B_{12} through a symbiotic relationship with bacteria. Nature 438:90–93

Cunha L, Grenha A (2016) Sulfated seaweed polysaccharides as multifunctional materials in drug delivery applications. Mar Drugs 14:42

Curson ARJ, Rogers R, Todd JD, Brearley CA, Johnston AWB (2008) Molecular genetic analysis of a dimethylsulfoniopropionate lyase that liberates the climate-changing gas dimethylsulfide in several marine α-proteobacteria and *Rhodobacter sphaeroides*. Environ Microbiol 10:757–767

De Clerck O, Kao SM, Bogaert KA, Blomme J, Foflonker F et al (2018) Insights into the evolution of multicellularity from the sea lettuce genome. Curr Biol 28:2921-2933.e5

Dhariwal A, Chong J, Habib S, King IL, Agellon LB, Xia J (2017) MicrobiomeAnalyst: a web-based tool for comprehensive

statistical, visual and meta-analysis of microbiome data. Nucleic Acids Res 45:W180

Dittami SM, Duboscq-Bidot L, Perennou M, Gobet A, Corre E, Boyen C, Tonon T (2016) Host-microbe interactions as a driver of acclimation to salinity gradients in brown algal cultures. ISME J 10:51–63

Dittami SM, Gravot A, Renault D, Goulitquer S, Eggert A, Bouchereau A, Boyen C, Tonon T (2011) Integrative analysis of metabolite and transcript abundance during the short-term response to saline and oxidative stress in the brown alga *Ectocarpus siliculosus*. Plant Cell Environ 34:629–642

Dominguez H, Loret EP (2019) *Ulva lactuca*, a source of troubles and potential riches. Mar Drugs 17:357

Edwards DM, Reed RH, Stewart WDP (1988) Osmoacclimation in *Enteromorpha intestinalis*: long-term effects of osmotic stress on organic solute accumulation. Mar Biol 98:467–476

Egan S, Harder T, Burke C, Steinberg P, Kjelleberg S, Thomas T (2013) The seaweed holobiont: understanding seaweed–bacteria interactions. FEMS Microbiol Rev 37:462–476

El-Sayed HS, Elshobary ME, Barakat KM, Khairy HM, El-Sheikh MA, Czaja R, Allam B, Senousy HH (2022) Ocean acidification induced changes in *Ulva fasciata* biochemistry may improve *Dicentrarchus labrax* aquaculture via enhanced antimicrobial activity. Aquaculture 560:738474

Emeline CB, Ludovic D, Laurent V, Catherine L, Kruse I, Erwan AG, Florian W, Philippe P (2021) Induction of phlorotannins and gene expression in the brown macroalga *Fucus vesiculosus* in response to the herbivore *Littorina littorea*. Mar Drugs 19:185

Estoup P, Gernigon V, Avouac A, Blanc G, Gobet A (2024) Exploring the influence of fertilization on bacterial community fluctuations in *Ulva* cultivation. Algal Res 82:130688

Ferrer A, Rivera J, Zapata C, Norambuena J, Sandoval Á, Chávez R, Orellana O, Levicán G (2016) Cobalamin protection against oxidative stress in the acidophilic iron-oxidizing bacterium *Leptospirillum* group II CF-1. Front Microbiol 7:748

Fichman Y, Gerdes SY, Kovács H, Szabados L, Zilberstein A, Csonka LN (2015) Evolution of proline biosynthesis: enzymology, bioinformatics, genetics, and transcriptional regulation. Biol Rev 90:1065–1099

Fox J, Weisberg S (2019) An R companion to applied regression (3rd ed). Sage Publications

Fraga CG, Croft KD, Kennedy DO, Tomás-Barberán FA (2019) The effects of polyphenols and other bioactives on human health. Food Funct 10:514–528

Geng N, Yang D, Hua J, Huang LJ, Dong H, Sun C, Xu L (2022) Complete genome sequence of *Kordiimonas pumila* N18T sheds light on biogeochemical roles of the genus *Kordiimonas*. Mar Genomics 62:100930

Ghaderiardakani F, Coates JC, Wichard T (2017) Bacteria-induced morphogenesis of *Ulva intestinalis* and *Ulva mutabilis* (Chlorophyta): a contribution to the lottery theory. FEMS Microbiol Ecol 93:fix094

Ghaderiardakani F, Quartino ML, Wichard T (2020) Microbiome-dependent adaptation of seaweeds under environmental stresses: a perspective. Front Mar Sci 7:575228

Giuffrè A, Borisov VB, Arese M, Sarti P, Forte E (2014) Cytochrome bd oxidase and bacterial tolerance to oxidative and nitrosative stress. Biochim Biophys Acta Bioenerg 1837:1178–1187

Glaeser SP, Kämpfer P (2014) The family Sphingomonadaceae. In: Rosenberg E, DeLong EF, Lory S, Stackebrandt E, Thompson F (eds) The Prokaryotes. Springer, Berlin, pp 641–707

González JM, Pinhassi J, Fernández-Gómez B, Coll-Lladó M, González-Velázquez M, Puigbò P, Jaenicke S, Gómez-Consarnau L, Fernàndez-Guerra A, Goesmann A, Pedrós-Alió C (2011) Genomics of the proteorhodopsin-containing marine flavobacterium *Dokdonia* sp. strain MED134. Appl Environ Microbiol 77:8676–8686

Groot Crego C, Hess J, Yardeni G, de La Harpe M, Priemer C, Beclin F, Saadain S, Cauz-Santos LA, Temsch EM, Weiss-Schneeweiss H, Barfuss MHJ, Till W, Weckwerth W, Heyduk K, Lexer C, Paun O, Leroy T (2024) CAM evolution is associated with gene family expansion in an explosive bromeliad radiation. Plant Cell 36:4109–4131

Hafting JT, Craigie JS, Stengel DB, Loureiro RR, Buschmann AH, Yarish C, Edwards MD, Critchley AT (2015) Prospects and challenges for industrial production of seaweed bioactives. J Phycol 51:821–837

Hardegen J, Amend G, Wichard T (2025) The microbiome of the seaweed cultivar *Ulva compressa* (Chlorophyta) and its persistence under micropollutant exposure. Environ Microbiol Rep 17:e70230

Hansen J, Møller I (1975) Percolation of starch and soluble carbohydrates from plant tissue for quantitative determination with anthrone. Anal Biochem 68:87–94

He Y, Hu C, Wang Y, Cui D, Sun X, Li Y, Xu N (2018) The metabolic survival strategy of marine macroalga *Ulva prolifera* under temperature stress. J Appl Phycol 30:3611–3621

Heric K, Maire J, Deore P, Perez-Gonzalez A, van Oppen MJH (2023) Inoculation with *Roseovarius* increases thermal tolerance of the coral photosymbiont, *Breviolum minutum*. Front Ecol Evol 11:1079271

Hmani I, Ghaderiardakani F, Ktari L, El Bour M, Wichard T (2024) High-temperature stress induces bacteria-specific adverse and reversible effects on *Ulva* (Chlorophyta) growth and its chemosphere in a reductionist model system. Bot Mar 67:131–138

Hoigné J, Bader H, Haag WR, Staehelin J (1985) Rate constants of reactions of ozone with organic and inorganic compounds in water—III. Inorganic compounds and radicals. Water Research 19:993–1004

Hong Z, Lakkineni K, Zhang Z, Verma DPS (2000) Removal of feedback inhibition of Δ1-pyrroline-5-carboxylate synthetase results in increased proline accumulation and protection of plants from osmotic stress. Plant Physiol 122:1129–1136

Hosseini SV, Dastgerdi HE, Tahergorabi R (2024) Marine mannitol: extraction, structures, properties, and applications. Processes 12:1613

Hudson J, Egan S (2022) Opportunistic diseases in marine eukaryotes: could Bacteroidota be the next threat to ocean life? Environ Microbiol 24:4505–4518

Hylleberg J (1975) Selective feeding by *Abarenicola pacifica* with notes on *Abarenicola vagabunda* and a concept of gardening in lugworms. Ophelia 14:113–137

Ingrisano R, Tosato E, Trost P, Gurrieri L, Sparla F (2023) Proline, cysteine and branched-chain amino acids in abiotic stress response of land plants and microalgae. Plants 12:3410

Jhunkeaw C, Khongcharoen N, Rungrueng N, et al (2021) Ozone nanobubble treatment in freshwater effectively reduced pathogenic fish bacteria and is safe for Nile tilapia (*Oreochromis niloticus*). Aquaculture 534:736286

Jiang J, Zhang X, Zhu X, Li Y (2017) Removal of intermediate aromatic halogenated DBPs by activated carbon adsorption: a new approach to controlling halogenated DBPs in chlorinated drinking water. Environ Sci Technol 51:3435–3444

Jimenez-Lopez C, Pereira AG, Lourenço-Lopes C, Garcia-Oliveira P, Cassani L, Fraga-Corral M, Prieto MA, Simal-Gandara J (2021) Main bioactive phenolic compounds in marine algae and their mechanisms of action supporting potential health benefits. Food Chem 341:128262

Jogler M, Chen H, Simon J, Rohde M, Busse HJ, Klenk HP, Tindall BJ, Overmann J (2013) Description of *Sphingorhabdus planktonica* gen. nov., sp. nov. and reclassification of three related members of the genus *Sphingopyxis* in the genus *Sphingorhabdus* gen. nov. Int J Syst Evol Microbiol 63:1342–1349

Joshi V, Joung JG, Fei Z, Jander G (2010) Interdependence of threonine, methionine and isoleucine metabolism in plants: accumulation and transcriptional regulation under abiotic stress. Amino Acids 39:933–947

Jung GY, Nam IH, Han YS, Ahn JS, Rhee SK, Kim SJ (2019) *Sphingorhabdus pulchriflava* sp. nov., isolated from a river. Int J Syst Evol Microbiol 69:2644–2650

Kakinuma M, Coury DA, Kuno Y, Itoh S, Kozawa Y, Inagaki E, Yoshiura Y, Amano H (2006) Physiological and biochemical responses to thermal and salinity stresses in a sterile mutant of *Ulva pertusa* (Ulvales, Chlorophyta). Mar Biol 149:97–106

Kalyuzhnaya MG, Bowerman S, Lara JC, Lidstrom ME, Chistoserdova L (2006) *Methylotenera mobilis* gen. nov., sp. nov., an obligately methelamine-utilizing bacterium within the family Methylophilaceae. Int J Syst Evol Microbiol 56:2819–2823

Kang I, Lim Y, Cho JC (2018) Complete genome sequence of *Granulosicoccus antarcticus* type strain IMCC3135T, a marine gammaproteobacterium with a putative dimethylsulfoniopropionate demethylase gene. Mar Genomics 37:176–181

Kessler RW, Weiss A, Kuegler S, Hermes C, Wichard T (2018) Macroalgal-bacterial interactions: role of dimethylsulfoniopropionate in microbial gardening by *Ulva* (Chlorophyta). Mol Ecol 27:1808–1819

Kirst GO, Thiel C, Wolff H, Nothnagel J, Wanzek M, Ulmke R (1991) Dimethylsulfoniopropionate (DMSP) in icealgae and its possible biological role. Mar Chem 35:381–388

Kits KD, Klotz MG, Stein LY (2015) Methane oxidation coupled to nitrate reduction under hypoxia by the Gammaproteobacterium *Methylomonas denitrificans*, sp. nov. type strain FJG1. Environ Microbiol 17:3219–3232

KleinJan H, Jeanthon C, Boyen C, Dittami SM (2017) Exploring the cultivable *Ectocarpus* microbiome. Front Microbiol 8:312517

Koblízek M, Janouškovec J, Oborník M, Johnson JH, Ferriera S, Falkowski PG (2011) Genome sequence of the marine photoheterotrophic bacterium *Erythrobacter* sp. strain NAP1. J Bacteriol 193:5881–5882

Kondrotaite Z, Valk LC, Petriglieri F, Singleton C, Nierychlo M, Dueholm MKD, Nielsen PH (2022) Diversity and ecophysiology of the genus OLB8 and other abundant uncultured Saprospiraceae genera in global wastewater treatment systems. Front Microbiol 13:917553

Kumari A, Kumar V, Ovadia R, Oren-Shamir M (2023) Phenylalanine in motion: a tale of an essential molecule with many faces. Biotechnol Adv 68:108246

Largo DB, Fukami K, Nishijima T, Ohno M (1995) Laboratory-induced development of the ice-ice disease of the farmed red algae *Kappaphycus alvarezii* and *Eucheuma denticulatum* (Solieriaceae, Gigartinales, Rhodophyta). J Appl Phycol 7:539–543

Lawrence MA (2016) ez: Easy analysis and visualization of factorial experiments (R package Version 4.4–0). https://cran.r -project.org/package=ez

Lenth RV (2021) Emmeans: Estimated Marginal Means, Aka Least-Squares Means. https://cran.r-project.org/package=emmeans

Li X, Blancheton JP, Liu Y, Triplet S, Michaud L (2014) Effect of oxidation-reduction potential on performance of European sea bass (*Dicentrarchus labrax*) in recirculating aquaculture systems. Aquacult Int 22:1263–1282

Liu X, Chen Y, Zhong M, Chen W, Lin Q, Du H (2019) Isolation and pathogenicity identification of bacterial pathogens in bleached disease and their physiological effects on the red macroalga *Gracilaria lemaneiformis*. Aquat Bot 153:1–7

Liu X, Zhang Y, Sun H, Tan S, Zhang XH (2023) Highly active bacterial DMSP metabolism in the surface microlayer of the eastern China marginal seas. Front Microbiol 14:1135083

Lomartire S, Cotas J, Pacheco D, Marques JC, Pereira L, Gonçalves AMM (2021) Environmental impact on seaweed phenolic production and activity: an important step for compound exploitation. Mar Drugs 19:245

Longmire JL, Maltbie M, Baker RJ, Museum TTU (1997) Use of "lysis buffer" in DNA isolation and its implication for museum collections. Museum of Texas Tech University, Lubbock

Love MI, Huber W, Anders S (2014) Moderated estimation of fold change and dispersion for RNA-seq data with DESeq2. Genome Biol 15:550

Lüder UH, Clayton MN (2004) Induction of phlorotannins in the brown macroalga *Ecklonia radiata* (Laminariales, Phaeophyta) in response to simulatęd herbivory - the first microscopic study. Planta 218:928–937

Lyon BR, Bennett-Mintz JM, Lee PA, Janech MG, Ditullio GR (2016) Role of dimethylsulfoniopropionate as an osmoprotectant following gradual salinity shifts in the sea-ice diatom *Fragilariopsis cylindrus*. Environ Chem 13:181–194

MacKeown H, Adusei Gyamfi J, Schoutteten KVKM, Dumoulin D, Verdickt L, Ouddane B, Criquet J (2020) Formation and removal of disinfection by-products in a full scale drinking water treatment plant. Sci Total Environ 704:135280

Mantri VA, Kazi MA, Balar NB, Gupta V, Gajaria T (2020) Concise review of green algal genus *Ulva* Linnaeus. J Appl Phycol 32:2725–2741

Mars Brisbin M, Schofield A, McIlvin MR, Krinos AI, Alexander H, Saito MA (2023) Vitamin B12 conveys a protective advantage to phycosphere-associated bacteria at high temperatures. ISME Commun 3:1–4

Martin M (2011) Cutadapt removes adapter sequences from high-throughput sequencing reads. Embnetj 17:10–12

Maxwell K, Johnson GN (2000) Chlorophyll fluorescence—a practical guide. J Exp Bot 51:659–668

McIlroy SJ, Nielsen PH (2014) The family Saprospiraceae. In: Rosenberg E, DeLong EF, Lory S, Stackebrandt E, Thompson F (eds) The Prokaryotes. Other Major Lineages of Bacteria and The Archaea. Springer, Berlin, pp 863–889

McKee LS, La Rosa SL, Westereng B, Eijsink VG, Pope PB, Larsbrink J (2021) Polysaccharide degradation by the Bacteroidetes: mechanisms and nomenclature. Environ Microbiol Rep 13:559–581

McMurdie PJ, Holmes S (2013) phyloseq: An R package for reproducible interactive analysis and graphics of microbiome census data. PLoS One 8:e61217

Muyzer G, De Waal EC, Uitterlinden AG (1993) Profiling of complex microbial populations by denaturing gradient gel electrophoresis analysis of polymerase chain reaction-amplified genes coding for 16S rRNA. Appl Environ Microbiol 59:695–700

Nedashkovskaya OI, Kukhlevskiy AD, Zhukova NV, Kim SB (2016) *Amylibacter ulvae* sp. nov., a new alphaproteobacterium isolated from the Pacific green alga *Ulva fenestrata*. Arch Microbiol 198:251–256

Negreanu-Pirjol T, Sirbu R, Mirea M, Negreanu-Pirjol BS (2020) Antioxidant activity correlated with chlorophyll pigments and magnesium content of some green seaweeds. Eur J Nat Sci Med 3:87–96

Nevarez-Flores E, Cruz-López R, Zertuche-González JA, Maske H, Ferreira-Arrieta A, Altamirano-Gómez Z, Sandoval-Gil JM (2024) Bacterial community dynamics on the seaweed *Ulva ohnoi* during a full cultivation cycle in a land-based aquaculture pond system. Algal Res 85:103847

Nguyen D, Ovadia O, Guttman L (2023) Temporal force governs the microbial assembly associated with *Ulva fasciata* (Chlorophyta) from an integrated multi-trophic aquaculture system. Front Microbiol 14:1223204

Nikitashina V, Stettin D, Pohnert G (2022) Metabolic adaptation of diatoms to hypersalinity. Phytochemistry 201:113267

O'Brien J, McParland EL, Bramucci AR, Ostrowski M, Siboni N, Ingleton T, Brown MV, Levine NM, Laverock B, Petrou K, Seymour J (2022) The microbiological drivers of temporally dynamic dimethylsulfoniopropionate cycling processes in Australian coastal shelf waters. Front Microbiol 13:894026

Oksanen JF, Blanchet G, Friendly M, Kindt R, Legendre P, McGlinn D, et al. (2020) vegan: Community Ecology Package (Version 2.5–7) [R package]. https://CRAN.R-project.org/package=vegan

Paula S, Volkov AG, Deamer DW (1998) Permeation of halide anions through phospholipid bilayers occurs by the solubility-diffusion mechanism. Biophys J 74:319–327

Pavia H, Brock E (2000) Extrinsic factors influencing phlorotannin production in the brown alga *Ascophyllum nodosum*. Mar Ecol Prog Ser 193:285–294

Pedregosa F, Varoquaux G, Gramfort A, Michel V, Thirion B, Grisel O, Blondel M, Müller A, Nothman J, Louppe G, Prettenhofer P, Weiss R, Dubourg V, Vanderplas J, Passos A, Cournapeau D, Brucher M, Perrot M, Duchesnay É (2012) Scikit-learn: machine learning in Python. J Mach Learn Res 12:2825–2830

Peña-Rodríguez A, Omont A, Quiroz-Guzmán E, Mendoza-Carrión G, García-Pérez OD, Elizondo-González R (2024) Microbiome changes of an integrated aquaculture system of shrimp *Litopenaeus vannamei* and seaweed *Ulva lactuca* with different water exchanges. Aquacult Int 32:1955–1973

Pettersson SJ, Lindholm-Lehto PC, Pulkkinen JT, Kiuru T, Vielma J (2022) Effect of ozone and hydrogen peroxide on off-flavor compounds and water quality in a recirculating aquaculture system. Aquacult Eng 98:102277

Phungsai P, Kurisu F, Kasuga I, Furumai H (2019) Molecular characteristics of dissolved organic matter transformed by O_3 and O_3/H_2O_2 treatments and the effects on formation of unknown disinfection by-products. Water Res 159:214–222

Pinheiro J, Bates D, DebRoy S, Sarkar D, R Core Team. (2018) nlme: linear and nonlinear mixed effects models. R Package Version 3.1–137. http://CRAN.R-project.org/package=nlme

Pintado J, Del Olmo G, Guinebert T, Ruiz P, Nappi J, Thomas T, Egan S, Masaló I, Cremades J (2023) Manipulating the *Ulva* holobiont: co-culturing *Ulva ohnoi* with *Phaeobacter* bacteria as a strategy for disease control in fish-macroalgae IMTA-RAS aquaculture. J Appl Phycol 35:2017–2029

Preiner J, Steccari I, Oburger E, Wienkoop S (2024) *Rhizobium* symbiosis improves amino acid and secondary metabolite biosynthesis of tungsten-stressed soybean (*Glycine max*). Front Plant Sci 15:1355136

Quast C, Pruesse E, Yilmaz P, Gerken J, Schweer T, Yarza P, Peplies J, Glöckner FO (2013) The SILVA ribosomal RNA gene database project: improved data processing and web-based tools. Nucleic Acids Res 41(:D590-D596

Ramírez-Puebla ST, Weigel BL, Jack L, Schlundt C, Pfister CA, Mark Welch JL (2022) Spatial organization of the kelp microbiome at micron scales. Microbiome 10:52

Rani G (2007) Changes in protein profile and amino acids in *Cladophora vagabunda* (Chlorophyceae) in response to salinity stress. J Appl Phycol 19:803–807

Reiser S, Schroeder JP, Wuertz S, Kloas W, Hanel R (2010) Histological and physiological alterations in juvenile turbot (*Psetta maxima*, L.) exposed to sublethal concentrations of ozone-produced oxidants in ozonated seawater. Aquaculture 307:157-164

Rezayian M, Niknam V, Faramarzi MA (2019) Antioxidative responses of *Nostoc ellipsosporum* and *Nostoc piscinale* to salt stress. J Appl Phycol 31:157–169

Saha M, Rempt M, Gebser B, Grueneberg J, Pohnert G, Weinberger F (2012) Dimethylsulphopropionate (DMSP) and proline from the surface of the brown alga *Fucus vesiculosus* inhibit bacterial attachment. Biofouling 28:593–604

Saha M, Rempt M, Stratil SB, Wahl M, Pohnert G, Weinberger F (2014) Defence chemistry modulation by light and temperature shifts and the resulting effects on associated epibacteria of *Fucus vesiculosus*. PLoS One 9:e105333

Sari-Chmayssem N, Taha S, Mawlawi H, Guégan JP, Jeftić J, Benvegnu T (2019) Extracted ulvans from green algae *Ulva linza* of Lebanese origin and amphiphilic derivatives: evaluation of their physico-chemical and rheological properties. J Appl Phycol 31:1931–1946

Saunders G, Kucera H (2010) An evaluation of rbcL, tufA, UPA, LSU and ITS as DNA barcode markers from the marine green macroalgae. Cryptogam Algol 31:487–528

Schmider E, Ziegler M, Danay E, et al (2010) Is It Really Robust?: Reinvestigating the Robustness of ANOVA Against Violations of the Normal Distribution Assumption. Methodology: Eur J Res Meth Behav Social Sci 6:147–151

Schroeder JP, Gärtner A, Waller U, Hanel R (2010) The toxicity of ozone-produced oxidants to the Pacific white shrimp *Litopenaeus vannamei*. Aquaculture 305:6–11

Schroeder JP, Reiser S, Croot PL, Hane R (2011) A comparative study on the removability of different ozone-produced oxidants by activated carbon filtration. Ozone Sci Eng 33:224–231

Scolding JWS, Powell A, Boothroyd DP, Shields RJ (2012) The effect of ozonation on the survival, growth and microbiology of the European lobster (*Homarus gammarus*). Aquaculture, 364–365:217–223

Shakya M, Silvester E, Rees G, Rajapaksha KH, Faou P, Holland A (2022) Changes to the amino acid profile and proteome of the tropical freshwater microalga *Chlorella* sp. in response to copper stress. Ecotoxicol Environ Saf 233:113336

Simon C, McHale M, Sulpice R (2022) Applications of *Ulva* biomass and strategies to improve its yield and composition: a perspective for *Ulva* aquaculture. Biology 11:1593

Singh RP, Reddy CRK (2014) Seaweed–microbial interactions: key functions of seaweed-associated bacteria. FEMS Microbiol Ecol 88:213–230

Singmann H, Bolker B, Westfall J, Aust F, Ben-Shachar M (2024) afex: Analysis of Factorial Experiments (Version 1.2–1) [R package]. https://CRAN.R-project.org/package=afex

Siripornadulsil S, Traina S, Verma DPS, Sayre RT (2002) Molecular mechanisms of proline-mediated tolerance to toxic heavy metals in transgenic microalgae. Plant Cell 14:2837–2847

Sitthi S, Mirutanaphai M, Satanwat P, Powtongsook S, Pungrasmi W (2024) Effect of ozone on *Vibrio* removal in a simulated earthen shrimp pond. Blue-Green Systems 6:310–326

Slobodkina G, Ratnikova N, Merkel A, Kevbrin V, Kuchierskaya A, Slobodkin A (2022) Lithoautotrophic lifestyle of the widespread genus *Roseovarius* revealed by physiological and genomic characterization of *Roseovarius autotrophicus* sp. nov. FEMS Microbiol Ecol 98:fiac113

Spoerner M, Wichard T, Bachhuber T, Stratmann J, Oertel W (2012) Growth and thallus morphogenesis of *Ulva mutabilis* (Chlorophyta) depends on a aombination of two bacterial species excreting regulatory factors. J Phycol 48:1433–1447

Steinhagen S, Enge S, Larsson K, Olsson J, Nylund GM, Albers E, Pavia H, Undeland I, Toth GB (2021) Sustainable large-scale aquaculture of the northern hemisphere sea lettuce, *Ulva fenestrata*, in an off-shore seafarm. J Mar Sci Eng 9:615

Steinhagen S, Larsson K, Olsson J, Albers E, Undeland I, Pavia H, Toth GB (2022) Closed life-cycle aquaculture of sea lettuce (*Ulva fenestrata*): performance and biochemical profile differ in early developmental stages. Front Mar Sci 9:942679

Summerfelt ST (2003) Ozonation and UV irradiation—an introduction and examples of current applications. Aquac Eng 28:21–36

Sunda W, Kieber DJ, Kiene RP, Huntsman S (2002) An antioxidant function for DMSP and DMS in marine algae. Nature 418:317–320

Szabados L, Savouré A (2010) Proline: a multifunctional amino acid. Trends Plant Sci 15:89–97

Teichberg M, Fox SE, Olsen YS, Valiela I, Martinetto P, Iribarne O, Muto EY, Petti MAV, Corbisier TN, Soto-Jiménez M, Páez-Osuna F, Castro P, Freitas H, Zitelli A, Cardinaletti M, Tagliapietra D (2010) Eutrophication and macroalgal blooms in temperate and tropical coastal waters: nutrient enrichment experiments with *Ulva* spp. Glob Change Biol 16:2624–2637

Toda K, Obolkin V, Ohira SI, Saeki K (2023) Abundant production of dimethylsulfoniopropionate as a cryoprotectant by freshwater phytoplanktonic dinoflagellates in ice-covered Lake Baikal. Commun Biol 6:1194

Tonon LAC, Moreira APB, Thompson F (2014) The family Erythrobacteraceae. In: Rosenberg E, DeLong EF, Lory S, Stackebrandt E, Thompson F (eds) The Prokaryotes. Alphaproteobacteria and Betaproteobacteria. Springer, Berlin, pp 213–235

Trigo JP, Engström N, Steinhagen S, Juul L, Harrysson H, Toth GB, Pavia H, Scheers N, Undeland I (2021) In vitro digestibility and Caco-2 cell bioavailability of sea lettuce (*Ulva fenestrata*) proteins extracted using pH-shift processing. Food Chem 356:129683

Tsugawa H, Cajka T, Kind T, Ma Y, Higgins B, Ikeda K, Kanazawa M, VanderGheynst J, Fiehn O, Arita M (2015) MS-DIAL: data-independent MS/MS deconvolution for comprehensive metabolome analysis. Nat Methods 12:523–526

Van Alstyne KL, Borgen N (2024) Seasonal effects of short-term stress on susceptibility to herbivores and DMSP induction in the intertidal green alga *Ulva fenestrata*. Mar Biol 171:86

Van Alstyne KL, Nelson TA, Ridgway RL (2015) Environmental chemistry and chemical ecology of "Green Tide" seaweed blooms. Integr Comp Biol 55:518–532

van der Loos LM, Steinhagen S, Stock W, Weinberger F, D'hondt S, Willems A, De Clerck O (2024) Functional stability despite high taxonomic turnover characterizes the *Ulva* microbiome across a 2,000 km salinity gradient. BioRxiv, 2024.06.20.599874.https://doi.org/10.1101/2024.06.20.599874

van der Loos LM, De Wilde C, Willems A, De Clerck O, Steinhagen S (2024b) The cultivated sea lettuce (*Ulva*) microbiome: successional and seasonal dynamics. Aquaculture 585:704692

van der Loos LM, D'hondt S, Engelen AH, Pavia H, Toth GB, Willems A, Weinberger F, De Clerck O, Steinhagen S (2023) Salinity and host drive *Ulva*-associated bacterial communities across the Atlantic–Baltic Sea gradient. Mol Ecol 32:6260–6277

van Grinsven S, Sinninghe Damsté JS, Harrison J, Polerecky L, Villanueva L (2021) Nitrate promotes the transfer of methane-derived carbon from the methanotroph *Methylobacter* sp. to the methylotroph *Methylotenera* sp. in eutrophic lake water. Limnol Oceanogr 66:878–891

Wang J, Tang X, Mo Z, Mao Y (2022) Metagenome-assembled genomes from *Pyropia haitanensis* microbiome provide insights into the potential metabolic functions to the seaweed. Front Microbiol, 13:857901

Weigel BL, Miranda KK, Fogarty EC, Watson AR, Pfister CA (2022) Functional insights into the kelp microbiome from metagenome-assembled genomes. MSystems 7(3):e0142221

Wellburn AR, Lichtenthaler H (1984) Formulae and program to determine total carotenoids and chlorophylls *a* and *b* of leaf extracts in different solvents. In: Sybesma C (ed) Advances in Photosynthesis Research. Springer, Dordrecht, pp 9–12

Wickham H (2016) ggplot2: Elegant Graphics for Data Analysis. Springer, New York

Wickham H, François R, Henry L, Müller K, Vaughan D (2023) dplyr: A Grammar of Data Manipulation (Version 1.1.4) [R package]. https://dplyr.tidyverse.org

Wichard T (2023) From model organism to application: bacteria-induced growth and development of the green seaweed *Ulva* and the potential of microbe leveraging in algal aquaculture. Semin Cell Dev Biol 134:69–78

Wichard T, Charrier B, Mineur F, Bothwell JH, De Clerck O, Coates JC (2015). The green seaweed *Ulva*: A model system to study morphogenesis. Front Plant Sci 6:123849

Xu X, He M, Xue Q, Li X, Liu A (2024) Genome-based taxonomic classification of the genus *Sulfitobacter* along with the proposal of a new genus *Parasulfitobacter* gen. nov. and exploring the gene clusters associated with sulfur oxidation. BMC Genom 25:389

Ye YQ, Hao ZP, Yue YY, Ma L, Ye MQ, Du ZJ (2022) Characterization of *Kordiimonas marina* sp. nov. and *Kordiimonas laminariae* sp. nov. and comparative genomic analysis of the genus *Kordiimonas*, a marine-adapted taxon. Front Mar Sci 9:919253

Yoon J, Matsuo Y, Kasai H, Yokota A (2012) *Portibacter lacus* gen. nov., sp. nov., a new member of the family Saprospiraceae isolated from a saline lake. J Gen Appl Microbiol 58:191–197

Yuan F, Yin S, Xu Y, Xiang L, Wang H, Li Z, Fan K, Pan G (2021) The richness and diversity of catalases in bacteria. Front Microbiol 12:645477

Zeng YX, Zhang YH, Li HR, Luo W (2020) Complete genome of *Sulfitobacter* sp. BSw21498 isolated from seawater of Arctic Kongsfjorden. Marine Genomics 53:100769

Zeroual S, El Bakkal SE, Mansori M, Lhernould S, Faugeron-Girard C, El Kaoua M, Zehhar N (2020) Cell wall thickening in two *Ulva* species in response to heavy metal marine pollution. Reg Stud Mar Sci 35:101125

Zhong Y, Xu J, Zhao X, Qu T, Guan C, Hou C, Tang X, Wang Y (2022) Balancing damage via non-photochemical quenching, phenolic compounds and photorespiration in *Ulva prolifera* induced by low-dose and short-term UV-B radiation. Int J Molec Sci 23:2693

Zhu X, Wang L, Lai Q, Wang J, Huang J, Li G, Zeng L, Xia J, Shao Z (2023) *Pseudophaeobacter profundi* sp. nov., isolated from the Western Pacific Ocean. Int J Systemat Evol Microbiol 73(9). https://doi.org/10.1099/ijsem.0.006071